frontiers in Earth Science

ORIGINAL RESEARCH
published: 22 January 2020
doi: 10.3389/feart.2019.00349

Raman Spectroscopy Detects Amorphous Carbon in an Enigmatic Egg From the Upper Cretaceous Wido Volcanics of South Korea

Seung Choi, Sung Keun Lee, Noe-Heon Kim, Seongyeong Kim and Yuong-Nam Lee**

School of Earth and Environmental Sciences, Seoul National University, Seoul, South Korea

Raman spectroscopy has been widely used in micropaleontology and organic geochemistry to identify carbonaceous materials and evaluate their thermal maturity in fossils or metasedimentary rocks. Meanwhile, fossil egg researches have mostly focused on biomineralized calcite, but preserved carbonaceous (or possibly organic) materials inside the eggshells have been usually neglected until recently. Here we report an enigmatic egg from the Wido Volcanics (Upper Cretaceous) of South Korea that was analyzed using diverse methods including polarized light microscope, scanning electron microscope, electron probe microanalyzer, electron backscatter diffraction, and Raman spectroscopy. The eggshell not only shows the crystallography of archosaurian eggshells but also contains peculiar dark bands, which were previously known as the trait of fossil and modern Crocodyliformes eggshells. Raman spectroscopic analysis showed that the dark bands are mainly due to amorphous carbon, as evidenced by the clear graphite (G) and disordered (D) bands. The deconvolution of amorphous carbon peaks and resultant parameters made it possible to infer the paleotemperature inscribed in the eggshell. The result suggests that preserved amorphous carbon in the fossil eggshells can be identified using Raman spectroscopy and Raman parameters may make it possible to compare the thermal maturity of spatiotemporally diverse fossil eggshells. The biogenicity of the dark band is not clear because Raman spectroscopic analysis is not sufficient to confirm biogenicity. However, overall distribution of the dark band may imply the biogenic origin. It is apparent that the material of this study is not a dinosaur egg but might belong to a crocodyliform or choristoderan egg, and even other non-dinosaur archosaur can be a candidate as well.

Keywords: Raman spectroscopy, amorphous carbon, thermal maturity, EBSD, fossil egg, Wido Volcanics, taphonomy

OPEN ACCESS

Edited by:
Paul Antony Selden,
University of Kansas, United States

Reviewed by:
Alison Olcott,
University of Kansas, United States
Graciela Helena Piñeiro,
Universidad de la República, Uruguay

****Correspondence:***
Seung Choi
seung0521@snu.ac.kr
Yuong-Nam Lee
ynlee@snu.ac.kr

Specialty section:
This article was submitted to Paleontology, a section of the journal Frontiers in Earth Science

Received: *22 September 2019*
Accepted: *16 December 2019*
Published: *22 January 2020*

Citation:
Choi S, Lee SK, Kim N-H, Kim S and Lee Y-N (2020) Raman Spectroscopy Detects Amorphous Carbon in an Enigmatic Egg From the Upper Cretaceous Wido Volcanics of South Korea. Front. Earth Sci. 7:349. doi: 10.3389/feart.2019.00349

INTRODUCTION

Along with diverse invertebrate fossils, vertebrate egg fossils are calcium carbonate-based biominerals (Mikhailov, 1997; Cusack and Freer, 2008; Pérez-Huerta et al., 2018). Calcium carbonate of fossil eggs not only provide reproductive paleobiological information of amniotes (Grellet-Tinner et al., 2006; Tanaka et al., 2015; Varricchio and Jackson, 2016 and references

therein; Choi et al., 2019; Yang et al., 2019) but also afford paleoenvironmental and taphonomic information overprinted in the eggs (Grellet-Tinner et al., 2010; Montanari et al., 2013; Angst et al., 2015; Moreno-Azanza et al., 2016; Graf et al., 2018; Kim et al., 2019; see also Montanari, 2018 and references therein). Modern avian eggshells are mostly composed of calcite (96%) with a rare amount of organic matrix (2%) and trace elements such as Mg, P, and S (Hincke et al., 2012; Dauphin et al., 2018). Likewise, modern crocodylian and (rigid) gecko eggshells are mostly composed of calcium carbonate in the form of calcite (Ferguson, 1982; Schleich and Kästle, 1988; Marzola et al., 2015; Choi et al., 2018) unlike turtle eggshells, which are mainly composed of aragonite (Lawver and Jackson, 2014). In all rigid eggshells of modern amniotes, organic materials are certainly a minor and easily degradable component so that they are rarely preserved in the fossil record (Hirsch, 1996, Table 2; Smith and Hayward, 2010). Accordingly, the majority of the fossil eggshell studies have focused on biominerals rather than preserved carbonaceous (potential organic) matters.

The reports on the potential preserved organic material of fossil eggs are, however, accumulating ever since the 1990s. For example, preserved shell membrane (membrana testacea; see Grellet-Tinner, 2005, Figure 1) was reported even from the Early Jurassic dinosaur eggs (e.g., Kohring and Hirsch, 1996; Kohring, 1999; Grellet-Tinner, 2005; Schweitzer et al., 2005; Stein et al., 2019). Unfortunately, many of the reports were merely based on the morphology of putative biological structure, thereby another line of evidence should be applied to guarantee the biogenicity of those structures (e.g., Schidlowski, 2001; Gupta et al., 2007; Stein et al., 2019; see also discussion of Schopf et al., 2005). On the other hand, Schweitzer et al. (2005) showed the presence of organic materials in the radial section of a titanosaur eggshell using an immunohistochemical approach, which is a superb tool to see a distribution of *in situ* organic materials and can identify the type of organic material using antigen-antibody reaction (but see also Saitta et al., 2018). Nevertheless, this approach requires rather complicated preparation steps and laboratory resources (see electronic appendix of Schweitzer et al., 2005) that are not easily available to most paleontologists.

In this respect, Raman spectroscopy used in Wiemann et al. (2018) and Yang et al. (2018) to detect preserved cuticle (an outermost proteinous layer of an eggshell) or pigments in the fossil eggshell is a promising technique because it is non-destructive and provides high spatial and spectral resolution without complicated preparation steps (Smith and Clark, 2004; Schweitzer et al., 2008; Olcott Marshall and Marshall, 2015). In addition, Raman spectroscopy is useful in appraising the thermal maturity of preserved organic materials (or at least carbonaceous material) in fossils (Hartkopf-Fröder et al., 2015; Olcott Marshall and Marshall, 2015 and references therein). By using the parameters derived from the Raman spectra of thermally matured carbonaceous materials, the preserved carbonaceous matter in metasedimentary rock samples (Beyssac et al., 2002; Rahl et al., 2005; Lahfid et al., 2010) or fossil fuels (Schito et al., 2017; Henry et al., 2019a) could be used as a 'thermometer' because the parameters are affected mainly by heat, but little affected by other variables such as pressure at least in higher metamorphic grade ($T > 350°C$) (Lahfid et al., 2010). The Raman spectroscopy, therefore, has been widely used by micropaleontologists and applied to diverse fossils including, but not limited to, acritarch (Marshall et al., 2005; Schiffbauer et al., 2012), conodont (Marshall et al., 2001; McMillan and Golding, 2019), foraminifera (McNeil et al., 2015), kerogenous microfossils (Schopf et al., 2005), plant spores (Bernard et al., 2007), and protist (Ferralis et al., 2016) to investigate the thermal maturity of those fossils. Although Raman spectroscopy does not fully prove the biogenicity of preserved carbonaceous matter in fossil and needs further confirmation by independent approaches (Pasteris and Wopenka, 2003; Marshall et al., 2010), Raman spectroscopy is the simplest tool to detect carbonaceous material in fossils, thus make further biogenicity test possible (Marshall et al., 2010). In fossil eggshells and vertebrate fossils in general, Raman spectroscopy has not been widely used except for a few pioneering studies (e.g., Piga et al., 2011; Thomas et al., 2011; Lee Y.C. et al., 2017), but as shown in Wiemann et al. (2018), Yang et al. (2018), and Stein et al. (2019), it has a great potential in vertebrate paleontology as it is in archeology (Smith and Clark, 2004).

In the fieldwork in 2016, a solitary partial egg had been found in the Wido Volcanics of South Korea where two types of dinosaur egg fossils were reported (Choi and Lee, 2019; Kim et al., 2019). The most peculiar microstructural feature of this egg is several parallel dark bands, which is reminiscent of the dark band structure in modern and fossil crocodyliform eggshells (e.g., Marzola et al., 2015; Russo et al., 2017). We hypothesized that the dark bands, which were observed in all eggshells, of this eggshell are attributed to the composition, mainly due to the preserved carbonaceous (probably organic) matter. Hence, the aim of this study is to provide a detailed description of a new egg using diverse analytical methods including Raman spectroscopy and to investigate the origin of the dark bands. Based on circumstantial evidence surrounding this fossil material and comparisons to modern crocodylian eggshells, we also deduced a possible egg-layer of this enigmatic egg.

GEOLOGICAL SETTING

The Wi Island is located in the Yellow Sea and a part of the successive Upper Cretaceous volcanic-influenced deposits in southwestern Korean Peninsula (**Figure 1A**; Chough et al., 2000; Kim S.W. et al., 2016; Choi and Lee, 2017, Figure 4; Kwon et al., 2017). The island is composed of the Wido Volcanics and can be further divided into four conformable subunits: Daeri Andesite, Mangryeongbong Tuff, Beolgeumri Formation, and Ttandallae Tuff in ascending order (**Figure 1B**; Koh et al., 2013; Ko et al., 2017). The Daeri Andesite is mostly composed of andesite but reddish mudstone layer with calcareous nodules lies at the bottom. This fossiliferous lithofacies was interpreted to be deposited in a floodplain under semi-arid paleoclimate (Gihm et al., 2017). The Mangryeongbong Tuff is mostly composed of massive lapilli tuff (Gihm and Hwang, 2014) and U-Pb radiometric age dating yielded 86.63 ± 0.83 Ma, which is the youngest age limit of the fossiliferous layer (Ko et al., 2017). The Beolgeumri Formation is composed of tuffaceous conglomerate,

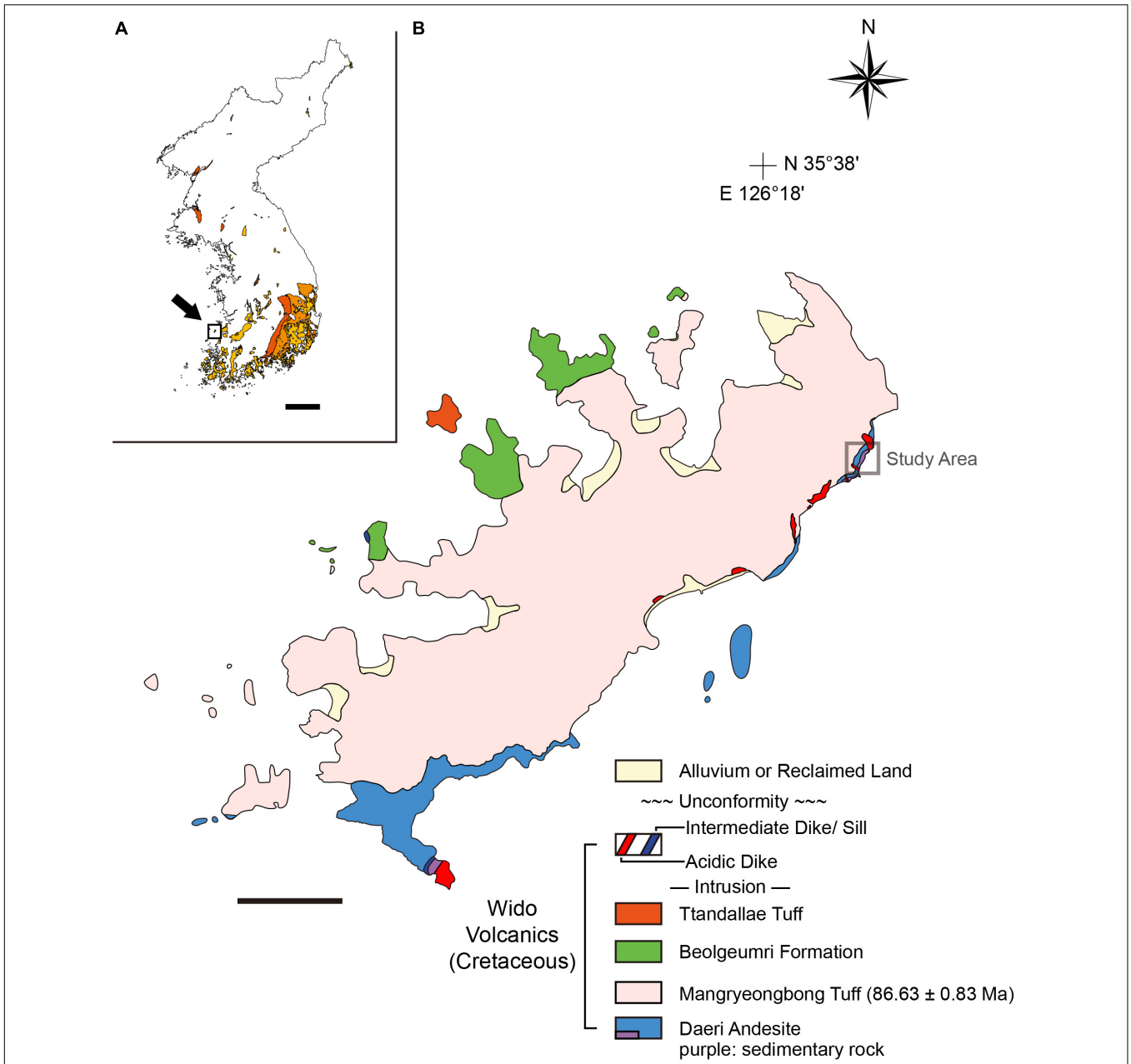

FIGURE 1 | Geological map of Wi Island, South Korea. **(A)** A map of the Korean Peninsula and distribution of the Cretaceous basins (colored regions). Note that Wi Island (inset square) is a part of volcanic-influenced sedimentary successions colored in yellow. Modified from Choi and Lee (2017). **(B)** A geological map of Wi Island. The Wido Volcanics is composed of four conformable units: Daeri Andesite, Mangryeongbong Tuff, Beolgeumri Formation, and Ttandallae Tuff in ascending order (Ko et al., 2017). Modified from Koh et al. (2013), Ko et al. (2017), and Choi and Lee (2019). Scale bars equal 100 km **(A)**; 1 km **(B)**.

coarse sandstone, very fine sandstone, and black shale (Koh et al., 2013; Ko et al., 2017). The Beolgeumri Formation was deposited in lacustrine environment that was highly influenced by the pyroclastic density currents triggered by earthquakes (Gihm and Hwang, 2014, 2016; Ko et al., 2017). The Ttandallae Tuff is the uppermost unit and composed of breccias and lapilli tuff, deposited from pyroclastic density currents (Ko et al., 2017).

The study area is in the lower part of the Daeri Andesite and characterized by siliciclastic mudstones with gravelly sandstones (Gihm et al., 2017; **Figure 2**). More specific geological characteristics of this area will be discussed in a separate paper and we will briefly present the locality information herein. In the north-eastern part of the study area, a few gravelly sandstone bodies of less than 2 m in thickness showing lenticular geometry are developed in the reddish mudstones. The sandstones are interpreted to have been deposited in ephemeral channels. The south-western part of the study area is dominated by mudstones containing numerous dinosaur eggs in clutches

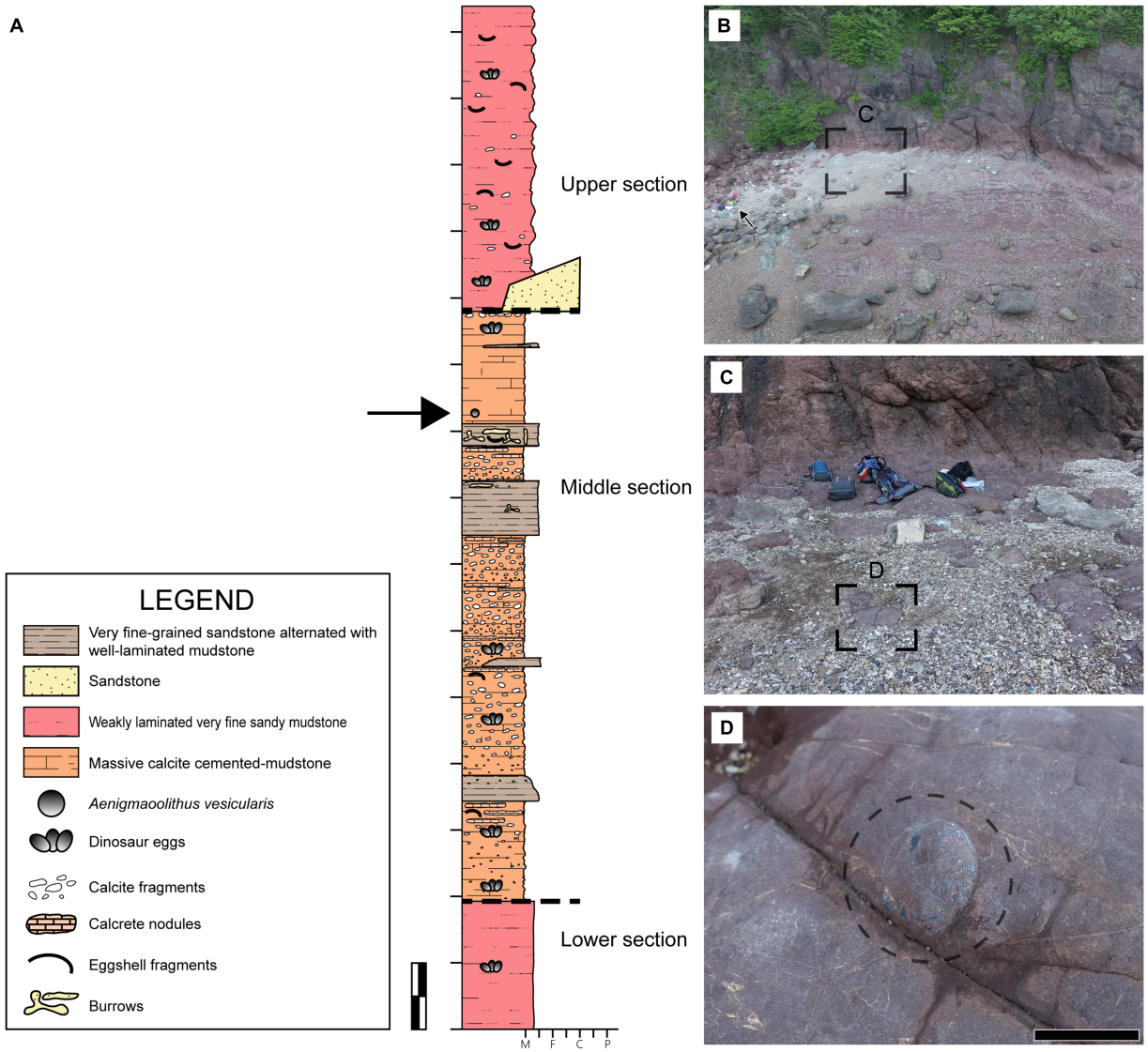

FIGURE 2 | Fossil locality. **(A)** A columnar section of the study area. It can be roughly divided into three sections based on the lithological and sedimentary characteristics. The lower and upper sections are composed of weakly laminated very fine sandy mudstones. The middle section is dominated by massive calcite cemented-mudstones and very fine-grained sandstone alternated with well-laminated mudstone. The deposits between the middle and the upper section are coarse to fine sandstones intercalated with mudstones, interpreted to have been deposited in crevasse splay. The stratigraphic position of the studying material is marked by a black arrow. M, F, C, and P stand for mud, fine sand, coarse sand, and pebble, respectively. **(B)** An aerial view of fossil locality. The material of this study was found near the upper end of horizontal outcrop. A green backpack for scale (a black arrow). **(C,D)** The material was found in an exposed siltstone. Scale bars equal 1 m **(A)**; 2 cm **(D)**.

(**Figure 2A**; mostly faveoloolithid eggs; Kim et al., 2019). The strata mainly composed of the mudstones are red in color, and the bedding geometry preserves original horizontality. In addition, the association of the deposits with channel sandstone bodies developed in the north-eastern part indicates that the study area was formed in a floodplain environment (Gihm et al., 2017). The sedimentary deposits of the study area can be largely divided into lower, middle and upper sections by sedimentary and pedogenic features (**Figure 2A**). The lithofacies of lower and upper sections are composed of weakly laminated very fine sandy mudstones. The middle section is characterized by massive calcite cemented-mudstone and very fine-grained sandstone alternated with well-laminated mudstone indicating sheet flooding deposits. The mudstone that contains clutches of dinosaur eggs in this section is massive, comprising finer sediments than those of the laminated sandy mudstones. Most of the primary sedimentary structures are faded out by weathering and/or pedogenesis. Bedded calcretes and rootlets are only developed in this lithofacies. All of these observations suggest that the reddish massive mudstones were formed in the more distal part of the floodplain with a lower sedimentation rate (Kraus, 1999).

MATERIALS AND METHODS

Materials

Only one incomplete egg of *Aenigmaoolithus vesicularis* oogen. et oosp. nov. (SNUVP 201701; **Figures 2B–D**) was found, but other ootaxa such as faveoloolithid *Propagoolithus widoensis* (Kim et al., 2019) and possible dromaeosaurid eggshell *Reticuloolithus acicularis* (Choi and Lee, 2019) were relatively abundant in the fossil locality. An incomplete egg was excavated in the field (**Figure 2D**). The four fragments were situated no more than 5 cm from the egg. The nearby eggshell fragments have dark bands exactly the same as those of the holotype egg, thus we used nearby fragments for physico-chemical analyses detailed below (**Figure 3A**) in order not to damage the holotype. The main microstructural features of holotype eggshell and nearby fragments are summarized in **Figure 3B**. See **Supplementary Figure S1** for further information.

Because the material is a definite archosaur egg (see EBSD observation below) but its microstructure is not similar to that of any known dinosaur (including Aves) eggshells (see section "Comparative Study" below), we analyzed eggshells of modern crocodile (*Caiman latirostris*, provided by Dr. Kohei Tanaka, University of Tsukuba, Japan) using selective methods for comparisons.

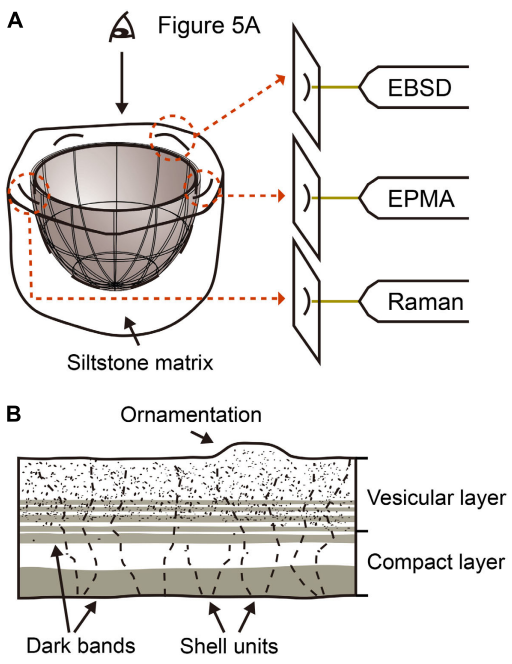

FIGURE 3 | Schematic view of study methods and eggshell microstructure. **(A)** The material excavated from the field is composed of partially preserved egg and nearby fragments. After confirming the consistent microstructure between the holotype and nearby fragments, the fragments were prepared for physico-chemical analyses. See also **Supplementary Figure S1**. **(B)** A schematic view and terminologies of microstructural features observed in both holotype egg and nearby fragments. See text for details.

Institutional Abbreviations

SNUVP, Paleontological Laboratory, Seoul National University, Seoul, South Korea; UHR, Hokkaido University Museum, Sapporo, Japan.

Polarized Light Microscopy (PLM)

Thin sections were made following the standard thin section preparation method of fossil eggshell (Quinn, 1994). The thin sections were observed and photographed using Nikon Eclipse LV100N POL, housed at the School of Earth and Environmental Sciences, Seoul National University (hereafter, SEES, SNU).

Scanning Electron Microscopy (SEM)

Freshly fractured radial sections were coated with carbon and examined using a JEOL JSM-7100F scanning electron microscope (SEM) (housed at SEES, SNU) with an accelerating voltage of 15.0 kV in secondary electron (SE) mode. In addition, lapped and polished materials used for EPMA and EBSD analyses were observed in the backscattered electron (BSE) mode. See Choi et al. (2018) for further detail.

Electron Probe Microanalyzer (EPMA) and Electron Backscatter Diffraction (EBSD)

Two eggshell fragments were lapped by hand with aluminum compounds with decreasing size, polished with 0.5 μm diamond paste, finalized with 0.06 μm colloidal silica, and coated with carbon. These specimens were used for chemical compositional analysis using field emission electron probe microanalyzer [FE-EPMA; JEOL JXA-8530F housed at the National Center for Inter-University Research Facilities (NCIRF), SNU] and crystallographic analysis using electron backscatter diffraction (EBSD; Oxford Instrument Symmetry detector attached to JEOL JSM-7100F in SEES, SNU). We acquired and curated EPMA (Choi et al., 2018; Kim et al., 2019) and EBSD data (Moreno-Azanza et al., 2013; Choi et al., 2019) following the established methods.

Raman Spectroscopy

Thin sections of the eggshells (SNUVP 201702 and *Caiman latirostris*) were analyzed using Raman spectroscopy. Raman spectroscopic analyses were performed in two steps. First, we applied Raman point-analysis in a radial section to get the spectra of the dark and plain parts of eggshell. In this step, we used a home-built micro Raman spectrometer (SEES, SNU) used in Kim E.J. et al. (2016) and Lee S.K. et al. (2017). The Raman spectra were collected using a laser wavelength of 488 nm, the laser power of 11 mW, and the exposure time of 2 s. The accumulation numbers of 60 and a grating groove density of 1800/500 lines mm^{-1} were used with 20X microscope objectives, and the estimated beam size is approximately 7.8 μm.

Secondly (applied only to SNUVP 201702), we performed Raman mapping analysis using DXR 2xi Raman Imaging Microscope (Thermo Fisher; NCIRF, SNU). The 2D Raman image of the specimen was constructed by measuring the intensity of the amorphous carbon peak at 1600 cm^{-1}. The

Raman signal was collected with beam size of ≥ 2.0 μm, a laser wavelength of 532 nm, and the laser power of 2.0 mW. Exposure time of 0.00625 s (160 Hz) with the number of scans of 50 were used. The image pixel size of 3.0 μm × 3.0 μm were used for capturing the total view of 300 μm × 300 μm.

As the Raman spectrum for the amorphous carbon consists typically of two peaks (i.e., graphite 'G' and disordered 'D' bands), the fraction of each band was obtained from deconvolution of the spectrum using Origin v.9.0. Note that these amorphous carbon peaks can be further deconvoluted (or decomposed) into several components. The consensus on numbers and types of the components is not conclusively made among the researchers (Henry et al., 2019b), but Sadezky et al. (2005) used four Lorentzian bands (G, D1, D2, and D4) at ∼1580, ∼1350, ∼1620, and ∼1200 cm^{-1}, respectively and a Gaussian band to G3 at ∼1500 cm^{-1} to simulate the Raman spectrum of amorphous carbon with good fit. The position of each band may shift with varying degree of thermal maturation of original carbonaceous precursor (Schito et al., 2017; Khatibi et al., 2019). In the current deconvolution similar peak positions for G, D1, D2, and D3 bands were used. We found that the D4 peak position of ∼1160 cm^{-1} can simulate the overall pattern of the spectrum better. As in Lahfid et al. (2010), the widths and positions were allowed to vary upon deconvolution.

The deconvolution of amorphous carbon peak yields full width at half maximum (FWHM), area (peak intensity), and height of each band. The relative peak intensity between these bands allowed us to roughly estimate the paleotemperature. For example, Beyssac et al. (2002) showed that the parameter named R2 [= D1 area/(G area + D1 area + D2 area)] can be used as a geothermometer in a higher metamorphic grade (paleotemperature range of 330–650°C). Likewise, Lahfid et al. (2010) proposed that another parameters RA1 and RA2 [RA1 = (D1 area + D4 area)/(G area + D1 area + D2 area + D3 area + D4 area)]; [RA2 = (D1 area + D4 area)/(G area + D2 area + D3 area)] may constrain temperature conditions relevant to advanced diagenesis to low-grade metamorphism (∼200–320°C). We note that the types of bands used in the earlier studies are somewhat different from those used in the current study (e.g., Voigt function, Beyssac et al., 2002; Lorentzian function, Lahfid et al., 2010). Therefore, the estimated temperature in the current study may provide a *rough* guide to the paleotemperature inscribed in our specimen.

SYSTEMATIC PALEONTOLOGY

Oofamily Incertae sedis.

Oogenus *Aenigmaoolithus* oogen. nov.

Type oospecies *Aenigmaoolithus vesicularis* oogen. et oosp. nov.

Diagnosis. As for the type and only oospecies.

Etymology. 'Aenigma,' Latin word of 'Enigma,' indicates unidentifiable affinity of an egg-layer and its peculiar microstructure compared to other known ootaxa; 'oo' and 'lithos' mean egg and stone in Greek, respectively.

Type locality and horizon. As for the type and only oospecies.

Oospecies *Aenigmaoolithus vesicularis* oogen. et oosp. nov.

Etymology. The specific name derived from abundant vesicles distributed in the eggshell.

Holotype. One partial egg (SNUVP 201701).

Referred specimens. One thin section for polarized light microscopy (PLM) and Raman spectroscopy investigation (SNUVP 201702), one fresh radial section for SE mode (SEM) observation (SNUVP 201703), and one polished section for FE-EPMA, EBSD, and BSE mode (SEM) observation (SNUVP 201704).

Type locality and age. Sedimentary deposits of the Daeri Andesite, Wido Volcanics, Wi Island of Buan County, North Jeolla Province, South Korea. Late Cretaceous [not younger than Santonian; older than 86.63 ± 0.83 Ma (Ko et al., 2017)].

Diagnosis. The outer surface is usually smooth but rarely nodular flat-topped ornamentation exists; thickness ranges from 178 to 214 μm (average 200 μm); shell units are wedge-shaped; large vesicles occupy outer half of the eggshell; dark bands composed of amorphous carbon exist mainly in the inner end of the eggshell (1/7–1/8 of the whole thickness of the eggshell) but also weakly exist in the middle part of the eggshell (see **Figure 3B**).

RESULTS

Taphonomic Consideration for Mineralized Part

Before detailed morphological description, we firstly present distribution of Mg in the eggshell because Mg might be related to potential disruption of original microstructure. In the experimental setting, Mg included 'artificial burial fluid (100 mM NaCl + 10 mM $MgCl_2$ aqueous solution)' combined with thermal treatment would effectively disrupt the original calcite grain shape in modern invertebrate shells compared to its control groups treated with thermal effects only or thermal effects with 'artificial meteoric fluid (10 mM NaCl aqueous solution)' (Casella et al., 2018).

In *A. vesicularis*, Mg showed characteristic bilaminar structure in that its concentration is lower in the inner part of the eggshell whilst the outer half (roughly equivalent to a vesicular layer in SEM observation; see below) is comparatively enriched with Mg (**Figure 4**). The sedimentary matrix also contains a high concentration of Mg. It is not certain whether detected Mg in the eggshell is endogenous or exogenous, but in the case of sympatric *Propagoolithus*, pore canals were filled with calcite enriched with Mg (Kim et al., 2019). Considering the porosity caused by the vesicles in the outer half of the eggshell (see SEM observation below), the outer half of *A. vesicularis* might be influenced by exogenous Mg.

Although the extent of thermal effect during the taphonomic history of the Wido Volcanics is unknown (but it is highly likely that thermal effect *per se* indeed existed; see below), the potential exogenous Mg (**Figure 4**; Kim et al., 2019) and extensive thermal effects that may be related to the volcanic activities or magmatism of the Wido Volcanics (Gihm and Hwang, 2014; Gihm et al., 2017) might have caused the favorable setting for the

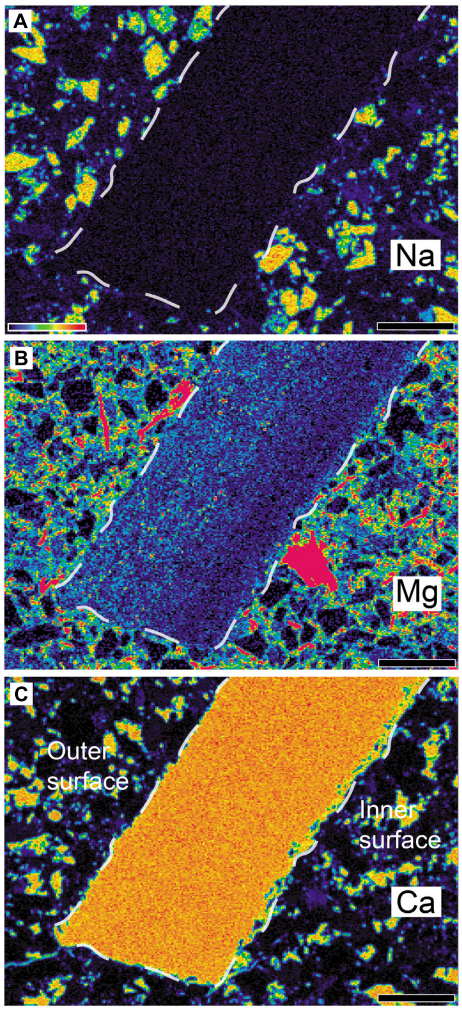

FIGURE 4 | Elemental composition of *Aenigmaoolithus vesicularis* oogen. et oosp. nov. (SNUVP 201704) and its surrounding matrix. **(A)** Na is nearly absent in the eggshell, whilst it is present in the matrix. **(B)** The concentration of Mg is somewhat higher in the outer half while it is nearly absent in the inner half. Mg is also highly enriched in the matrix. **(C)** The concentration of Ca is very high in the eggshell as well as some parts of the matrix. A colored-bar in **(A)** shows the intensity of the signal with red represents a stronger one. Note that the panels do not share absolute concentration scale. The eggshell boundaries are marked by white dashed lines. All scale bar equals 100 μm.

degradation of calcite grains (Casella et al., 2018) at the outer half of the eggshell.

Thus, the preservation of horizontal layering in the inner part of the eggshell and its weakening toward the outer surface (see SEM observation below) may be affected by taphonomic process so that they should be considered in observation. See also **Supplementary Figure S2** for the distribution of P and S.

Macroscopic

A cross-section of an egg is exposed (**Figures 5A,B**). Its diameter ranges from 21 to 23 mm. There are many eggshell fragments inside the only fragmentary egg. Almost all fragments are cut to expose their radial section but only one fragment exposes its inner surface. The external surface of the egg is not exposed. In general, accumulated fragments of a crushed egg are usually located at the bottom of an egg (Mueller-Töwe et al., 2002; Grigorescu, 2017), thereby the specimen may represent a bottom cross-section of an egg. Eggshell fragments juxtaposed within the outline of the egg are parallel to the curvature but those inside are randomly arranged and concentrated in one part of the section.

The eggshell is very thin (200 μm in average thickness; see PLM observation below), suggesting a small egg size because the eggshell thickness and egg mass have a positive correlation (Ar et al., 1979) and it is also certain that the egg mass is positively correlated with the egg size. Among the fossil eggs of which intact size and thickness are reported, *Sankofa pyrenaica* (theropod egg) is 270 μm in average thickness and is 7 cm × 4 cm in size (López-Martínez and Vicens, 2012), which is comparable to *A. vesicularis* on its thinness. Thus, the original size of *A. vesicularis* would be smaller than that of *Sankofa pyrenaica*.

Polarized Light Microscopy

The outer surface of the eggshell is smooth without noticeable ornamentation in radial view (but see SEM observation below). The thickness of eggshell ranges from 178 to 214 μm with an average of 200 μm. Under normal light, at least four layers stand out based on color variation: darkest inner band; translucent band; a pale dark band that has intermittent translucent bands within it; translucent band in the remaining external part of the eggshell (**Figure 5C**). The eggshell shows columnar to wedge-like extinction pattern under the polarized light (**Figure 5D**). In some parts, however, the extinction pattern is irregular. It should be noted that the extinction pattern is similar to the grain shape of calcite detected by EBSD analysis (Athanasiadou et al., 2018; see EBSD observation below) that was also reported in non-avian dinosaur eggshell fossils (e.g., see Moreno-Azanza et al., 2013, Figures 1, 3 for cases of *Trigonoolithus amoae* and cf. *Maiasaura* eggshell) and extant gecko eggshells (Choi et al., 2018, Figures 4, 9).

Scanning Electron Microscopy

We present SEM imaging with two approaches: secondary electron (SE) imaging using freshly fractured eggshell and BSE imaging using lapped and polished eggshell. Under SE mode, the overall morphology is not very characteristic, but columnar structures are often observed in the inner part of the eggshell (**Figures 6A,B**). The length of the preserved columns varies but the width is uniform (9.43–12.4 μm with an average of 11.1 μm). Each column and the inner half of the entire eggshell show horizontally stacked crystalline layers. The layering becomes weaker toward the outer surface, but it may be an artifact caused by taphonomic influences (see Taphonomic consideration above). In some cases, exposed section of a calcite layer shows numerous vesicle-like structures with varying sizes (**Figure 6C**). In a few cases, horizontal or slightly inclined gully-like structures are seen (**Figure 6D**), which might be the trace of dissolved organic fiber (e.g., see Choi et al., 2018,

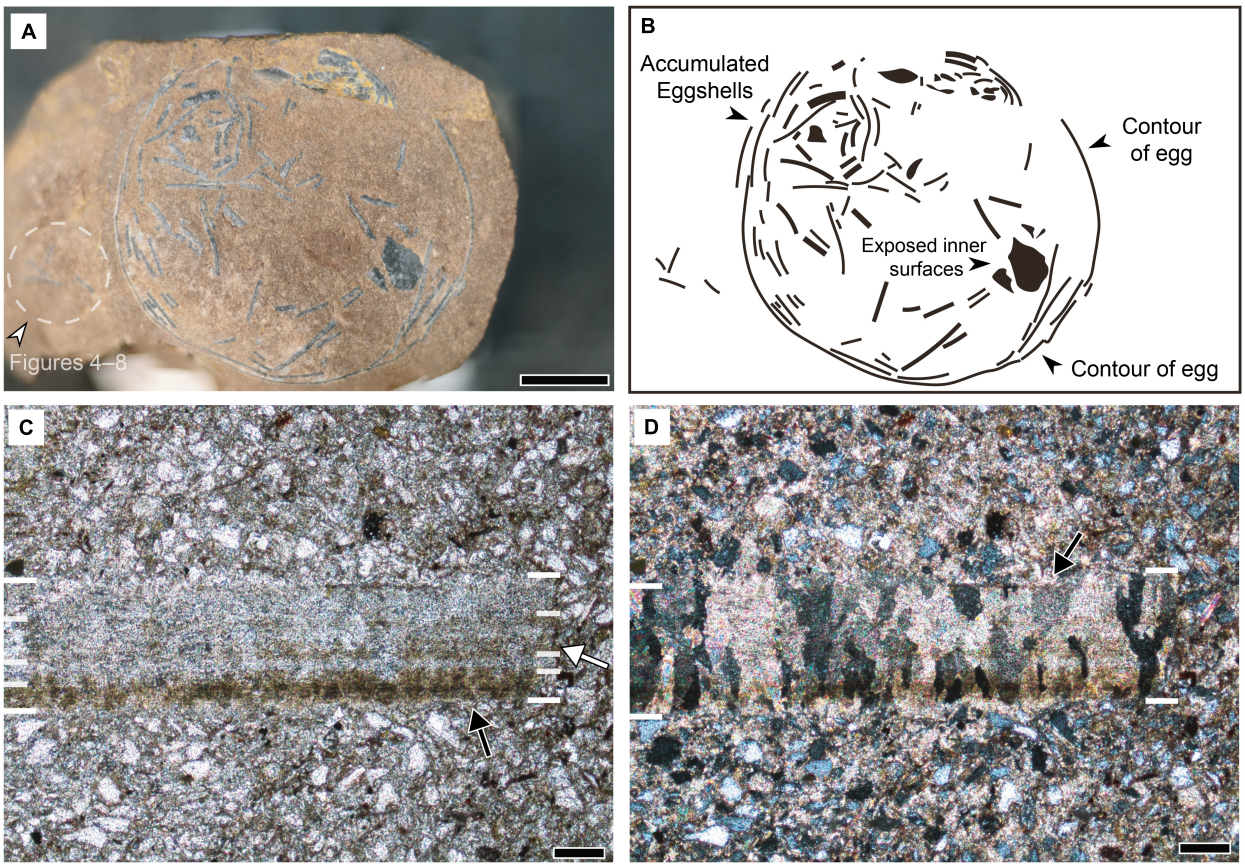

FIGURE 5 | Macroscopic and microstructural features of *Aenigmaoolithus vesicularis* oogen. et oosp. nov. **(A)** A cross-section of the holotype (SNUVP 201701). The eggshell fragments nearby the holotype (a white arrowhead and dashed circle) are used for physico-chemical analyses. **(B)** A schematic view of the holotype egg. **(C)** PLM view under normal light (SNUVP 201702). At least four layers are identified: innermost dark band (a black arrow), inner translucent layer, middle pale dark band (a white arrow), and outer translucent layer. The boundaries are marked by white bars. **(D)** PLM view under polarized light (SNUVP 201702). Extinction pattern is irregular, columnar, and wedge-like (a black arrow). Scale bars equal 5 mm **(A)**; 100 μm **(C,D)**.

Supplementary Figures S2I–L). The width of this structure is consistent with that of large vesicles.

In BSE imaging, two sublayers are prominent. The inner half (compact layer; CL in **Figures 6E,F,H**) is filled with very minute vesicles. The bigger vesicles are very rare in this layer. In outer half (vesicular layer; VL in **Figures 6E,G,H**) of the eggshell, larger vesicles are abundant, but minute vesicles are also present between the larger vesicles. The length ranges of larger and very minute vesicles are 0.910–4.520 μm (2.108 μm in average) and 0.110–0.454 μm (0.304 μm in average), respectively. On the other hand, the ornamentation-like structure was observed at one point on the external surface (**Figure 6H**). The ornamentation-like structure was morphologically similar to that reported in authentic choristoderan eggshell that is nodular and flat-topped in shape (Hou et al., 2009). It contains larger vesicles as in the vesicular layer lying below, supporting the biogenicity of this structure. Therefore, we interpret it as a genuine ornamentation rather than a taphonomic artifact (e.g., epitaxial diagenetic calcite growth). Except for this ornamentation, the external surface is smooth (see PLM observation above) and uniform in thickness. Considering the fact that non-ornamented plain parts of the eggshell have consistent thickness (e.g., Choi et al., 2018, 2020), it also supports the non-taphonomic origin of ornamentation structure described herein.

Electron Backscatter Diffraction

Electron backscatter diffraction imaging shows that the calcite grains with horizontal *c*-axis are present in the inner part of eggshell whereas *c*-axis align vertically toward the outer surface (**Figure 7A**). As seen from the extinction pattern (see PLM observation above), the shell units are usually wedge-like (**Figures 7A–C**), a feature also known in modern and fossil crocodyliform eggshells (see Hirsch and Quinn, 1990; Tanaka et al., 2011; Moreno-Azanza et al., 2014a, 2015; Marzola et al., 2015, Table 3; Srivastava et al., 2015; Jackson and Varricchio, 2016; Russo et al., 2017). One may think that the calcite grains with horizontal *c*-axis are diagenetic calcites, but the extant crocodyliform eggshells also show calcite with horizontal *c*-axis to the middle part of the eggshell (see "Comparative Study" below). Furthermore, in case when diagenetic calcites grow in the empty space in the eggshell, they are usually chaotic in

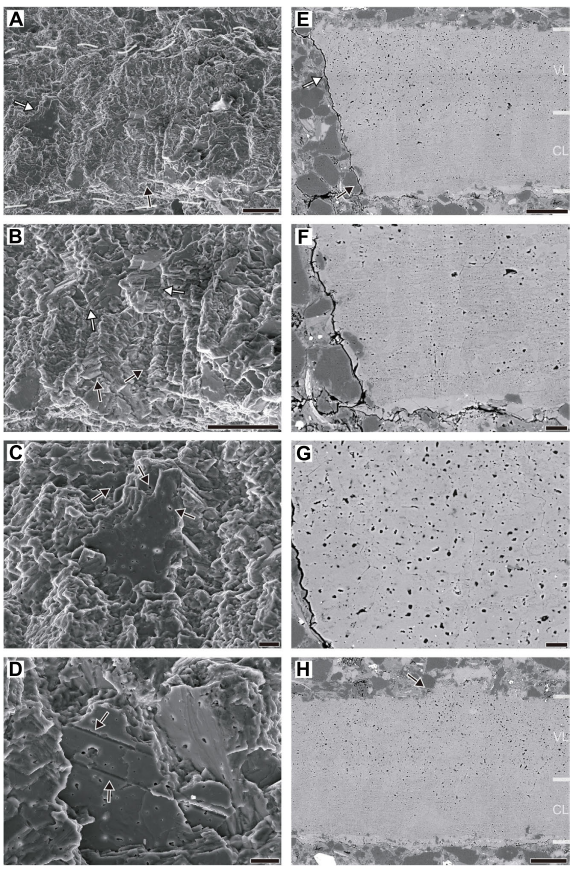

FIGURE 6 | Ultrastructural features of *Aenigmaolithus vesicularis* oogen. et oosp. nov. **(A–D)** Secondary electron imaging (SNUVP 201703). **(A)** A fresh section. The boundaries of the eggshell are marked by dashed lines. The columnar structure is observed in the inner part (a black arrow). Occasionally, a section of the calcite plates composing the eggshell is exposed (a white arrow). **(B)** A detailed view of columnar structure. Note columnar structures (black arrows) and stacked calcite plates (white arrows). **(C)** A detailed view of an exposed calcite plate. Abundant vesicles are observed in the section and other parts of the eggshell (black arrows). **(D)** "Gully-like" structures exposed in calcite plates. The widths of "gully" are consistent with the diameter of larger vesicles. **(E–H)** Backscattered electron imaging (SNUVP 201704). **(E)** A polished section. Note the two layers: a compact layer (CL; a black arrow) and a vesicular layer (VL; a white arrow). **(F)** In CL, calcite contains very minute vesicles whereas large vesicles are uncommon. **(G)** In VL, larger vesicles are dominant but very minute vesicles are also present between the larger vesicles. **(F)** and **(G)** are in the same magnification. **(H)** Rarely, ornamentations are present at the outer surface of eggshell (a black arrow). Note the existence of larger vesicles in the ornamentation. Scale bars equal 50 μm **(A,B,E,H)**; 10 μm **(C,D,F,G)**.

their crystallographic orientation or epitaxial to adjacent calcites (Moreno-Azanza et al., 2016; Kim et al., 2019). Moreover, the diagenetic calcite growth could be differentiated by the high concentration of Mg compared to that of the eggshells in Wi Island eggshell fossils (Kim et al., 2019), but this phenomenon was not observed in *A. vesicularis* (**Figure 4B**). Hence, the calcite with horizontal *c*-axis in *A. vesicularis* would be a biological trait. The grain boundaries are usually high-angled (>20°; **Figures 7C,F**).

In the ornamentation, the grains constituting the ornamentation are continuous with respect to the underlying main body of the eggshell (**Figures 7D,E**). This observation supports the biogenicity of the ornamentation unless it was made by the epitaxial growth of calcites (i.e., diagenetic overgrowth; Moreno-Azanza et al., 2016; Choi et al., 2019, 2020; Kim et al., 2019). However, the epitaxy is highly unlikely considering the presence of larger vesicles inside the ornamentation (**Figures 7D–F**; see SEM observation above).

Raman Spectroscopy

The eggshell is embedded in the siltstone matrix that consists mainly of quartz grains (**Figure 8A**). Raman spectra were acquired at the dark band and plain part of the eggshell. The plain part shows the peaks at 1087, 713, 282, and 156 cm^{-1} (**Figure 8B** and **Supplementary Figure S3**), correspond to the characteristic vibrational modes of calcite (Yang et al., 2018; Stein et al., 2019, Supplementary Figure S2). The Raman spectrum collected at the dark band (with label "C" in **Figure 8A**) near the inner edge of the eggshell revealed the broad peaks at 1340–1360 cm^{-1} (D band) and 1580–1620 cm^{-1} (G band), along with the 1087 cm^{-1} calcite peak, respectively (**Figure 8C** and **Supplementary Figure S3**). The doublet-like feature corresponds uniquely to disordered amorphous carbon (e.g., Tuinstra and Koenig, 1970; Ferrari and Robertson, 2000; Sadezky et al., 2005 and references therein). The results confirm that the dark band at the inner edge of the eggshell consists mainly of amorphous carbon. While the dark band is prevalent near the inner edge of the eggshell, it also exits throughout the eggshell as evidenced from the distribution of dark spots (**Figure 8A**).

We further acquired the distribution of amorphous carbon throughout the selected area of eggshell by measuring the peak intensity of the G band (1600 cm^{-1}) (**Figures 8A,D**). The resulting 2D image shows that the inner dark band is indeed rich in amorphous carbon compared to the other parts of the eggshell (**Figure 8D**). The image also confirmed the non-negligible presence of amorphous carbon throughout the eggshell, while the intensity is much less. The distribution patterns confirm that dark bands in the eggshell are attributable to amorphous carbon (**Figures 5B**, **8D**). The matrix outside the eggshell composed of siliciclastic sediments (Kim et al., 2019, Supplementary Figure S5) shows very low amorphous carbon signal (**Figure 8D**).

The fractions of G and D peaks were obtained based on the deconvolution method of Sadezky et al. (2005) (see section "Materials and Methods" above). The deconvolution result indeed confirmed that the experimental Raman spectrum can be well-described with five (G, D1, D2, D3, and D4) Raman bands (**Figure 9A**). We also obtained the fraction of each band using the deconvolution protocol by Lahfid et al. (2010; All Lorentzian) but this result was not as good as the former (**Figure 9B**). While the difference in the fractions of each band is not significant, we used the former method to estimate the fractions of 5 bands. The parameters acquired by the deconvolution are presented in **Table 1**.

The estimated Raman parameters (**Table 1**) were used to infer the paleotemperature using the band-based geothermeters (e.g., for higher metamorphic grade, T > 350°C; Beyssac et al., 2002;

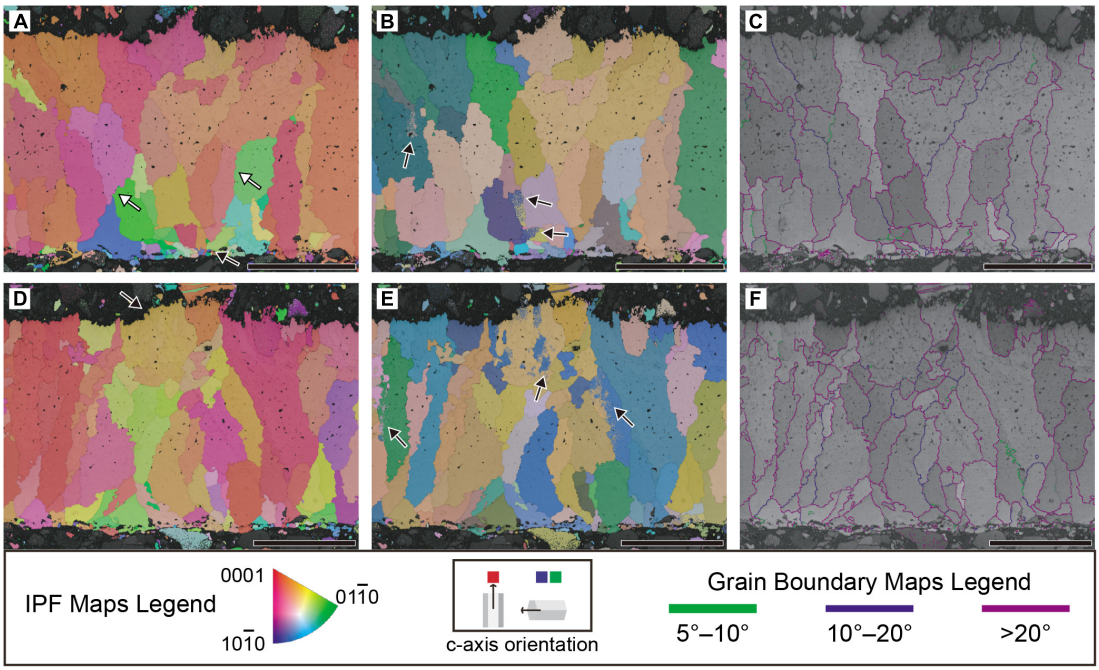

FIGURE 7 | Crystallography of *Aenigmaoolithus vesicularis* oogen. et oosp. nov. (SNUVP 201704). **(A,D)** Inverse pole figure (IPF) maps; **(B,E)**, Euler maps; **(C,F)**, grain boundary maps. In IPF maps, when *c*-axis of a calcite grain lies perpendicular to the eggshell surface, it is colored red. When lies parallel to the eggshell surface, it is colored green or blue. In Euler map, different grains have a different color so that it is easy to differentiate calcite grains. In grain boundary maps, boundary angle 5°–10° is colored green, 10–20° dark purple, and >20° light purple. In **(A)**, note wedge-like shell units marked by white arrows. The radiating calcite grains in the inner end are very similar to a mammillary layer of archosaur eggs (a black arrow in **A**). An ornamentation is marked by a black arrow in **(D)**. Note the crystallographic continuity between the ornamentation and underlying eggshell. In **(B,E)**, the color gradation marked by black arrows is limitation of visual representation of Euler map, not a biological phenomenon, thus crystallographically insignificant. **(C,F)** Most grain boundaries are higher than 20°. All scale bars equal 100 μm.

and lower metamorphic grade temperature conditions, 200°C < T < 320°C; Lahfid et al., 2010). **Table 2** summarizes the estimated paleotemperature. Based on the geothermometer for high temperature conditions (Beyssac et al., 2002), the estimated paleotemperature is ∼320°C, which is lower than the lower limit of the system (350°C). Based on another geothermometer (Lahfid et al., 2010), the estimated paleotempertuare is ∼360°C, which is higher than the higher limit of the system (320°C). It may be caused by the different deconvolution methods adopted in Beyssac et al. (2002) and Lahfid et al. (2010) compared to ours (Sadezky et al., 2005), or the lower estimation power at the margin of each system. Nevertheless, the values obtained from both estimations are roughly similar. Therefore, the paleotemperature inscribed in *A. vesicularis* from the Wido Volcanics would be *roughly* 340 ± 30°C. This temperature is sufficient to burn avian feathers into a complete black ash (Saitta et al., 2018, Supplementary Figures S142, S143).

COMPARATIVE STUDY

With a Modern Crocodylian Eggshell

Because *A. vesicularis* shows Crocodylia-eggshell-like shell unit structure under EBSD analysis and dark banded structure, but it is no similar to any known EBSD mapping images of dinosaur eggshells (Choi et al., 2019, Table 1), we further analyzed a modern crocodylian eggshell (*Caiman latirostris*) using EBSD, BSE mode of SEM, and Raman spectroscopy (**Figure 10**). We found several similarities between the modern crocodylian eggshell and *A. vesicularis*, but at the same time, we could find notable differences.

Crystallography of *Caiman latirostris* Eggshell

The crystallography of *Caiman latirostris* eggshell revealed by EBSD analysis shows that, to some extent, it is composed of calcite with horizontal *c*-axis at the inner part of the eggshell, whereas the outer part is mainly composed of vertically aligned larger calcite grains (**Figures 10A,B**). This overall configuration is consistent with that of other archosaur eggshells (Silyn-Roberts and Sharp, 1986; Packard and DeMarco, 1991; Lawver and Jackson, 2014; Choi et al., 2019, Table 1) but completely different from that of gekkotan (Squamata) eggshells (Choi et al., 2018). However, compared with dinosaur eggshells, each calcite grain composing *Caiman latirostris* eggshell has a relatively larger portion in the whole thickness of an eggshell. In addition, *Caiman latirostris* eggshell unit is usually wedge-shaped in radial view and the grains with horizontal *c*-axis occupy to the middle of the eggshell (**Figure 10B**) as in *A. vesicularis*. The latter trait has never been observed in non-neognath dinosaur eggshells (Choi et al., 2019, Table 1 and references therein). Although modern neognath eggshells have a large portion of calcite

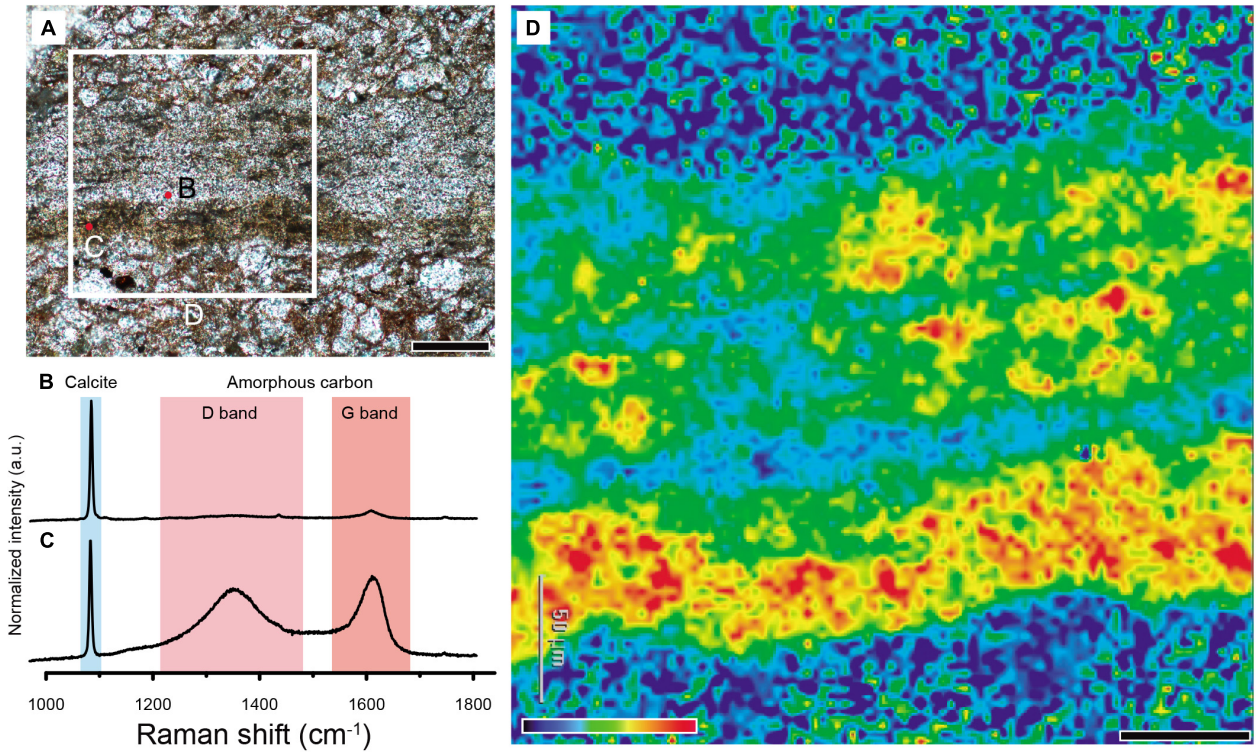

FIGURE 8 | Detection of amorphous carbon in *Aenigmaoolithus vesicularis* oogen. et oosp. nov. **(A)** An analyzed thin section (SNUVP 201702). Point analysis was carried out in the translucent region and a dark band (marked by red dots), respectively. The mapped region is marked by a white square. **(B)** The Raman spectrum acquired at the translucent region. Note calcite peak and very weakly developed G band. **(C)** The Raman spectrum acquired at the dark band. Note well-developed (G,D) bands as well as calcite peak. **(D)** The Raman mapping of the eggshell. The detecting frequency was set on the 1600 cm^{-1} (G band). Note the dark band in the inner end of the eggshell is highly enriched with amorphous carbon. Scale bars equal 100 µm **(A)**; 50 µm **(D)**.

with horizontally laid *c*-axis, they are often extended to the external surface of the eggshell (Choi et al., 2019, Figure 1). Thus, the pattern of neognath eggshells is different from that of modern crocodylian eggshells of which the grains with horizontal *c*-axis is usually confined to the middle of the eggshells (**Figure 10B**). These observations support that, to our knowledge, *A. vesicularis* has a crystallographic similarity with crocodyliform eggshells among the known archosaur eggshells.

Raman Spectroscopy of *Caiman latirostris* Eggshell

In contrast, the dark band of *Caiman latirostris* eggshells does not show clear evidence for the presence of amorphous carbon, which is observed in *A. vesicularis*. Some earlier studies have shown that modern crocodylian eggshells are characterized by the existence of dark bands at the inner end and the middle of thin section images (e.g., Fernández et al., 2013; Marzola et al., 2015, Figure 13). They were usually explained as the existence of organic matter (e.g., Marzola et al., 2015). To test whether amorphous carbon detected in *A. vesicularis* is observed in modern crocodylian eggshells, we applied Raman spectroscopy at the inner end of the *Caiman latirostris* eggshell where the eggshell is usually dark in thin section imaging (**Figure 10E**). The result showed that the Raman spectrum only shows the calcite peak (**Figure 10G**) similar to the plain part of the eggshell lying above (**Figure 10F**). It means that the dark band at the inner end of the modern crocodylian eggshell is not caused by the amorphous carbon unlike *A. vesicularis*. Alternatively, some pristine organic matter (i.e., not thermally matured ones) may be present here as suggested in Marzola et al. (2015) that may be detected by Fourier-transform infrared spectroscopy (FTIR), useful to detect functional groups of pristine organic matter (Olcott Marshall and Marshall, 2015). Potential pristine organic matter may cause the dark tint present in modern crocodyliform eggshells, but testing this hypothesis was out of scope of the present study.

BSE Mode Observation of *Caiman latirostris* Eggshell

On the other hand, the BSE imaging shows that the inner end of the *Caiman latirostris* eggshell is composed of porous calcite (**Figures 10C,D**), which is well-consistent with the inner dark part in thin section images (compare **Figures 10C,E**). We think, therefore, that the inner dark part of the modern crocodylian eggshell is mostly caused by the porosity of the calcified eggshell.

In the case of the dark band at the middle of crocodylian eggshell, unfortunately, the material of this study (*Caiman*

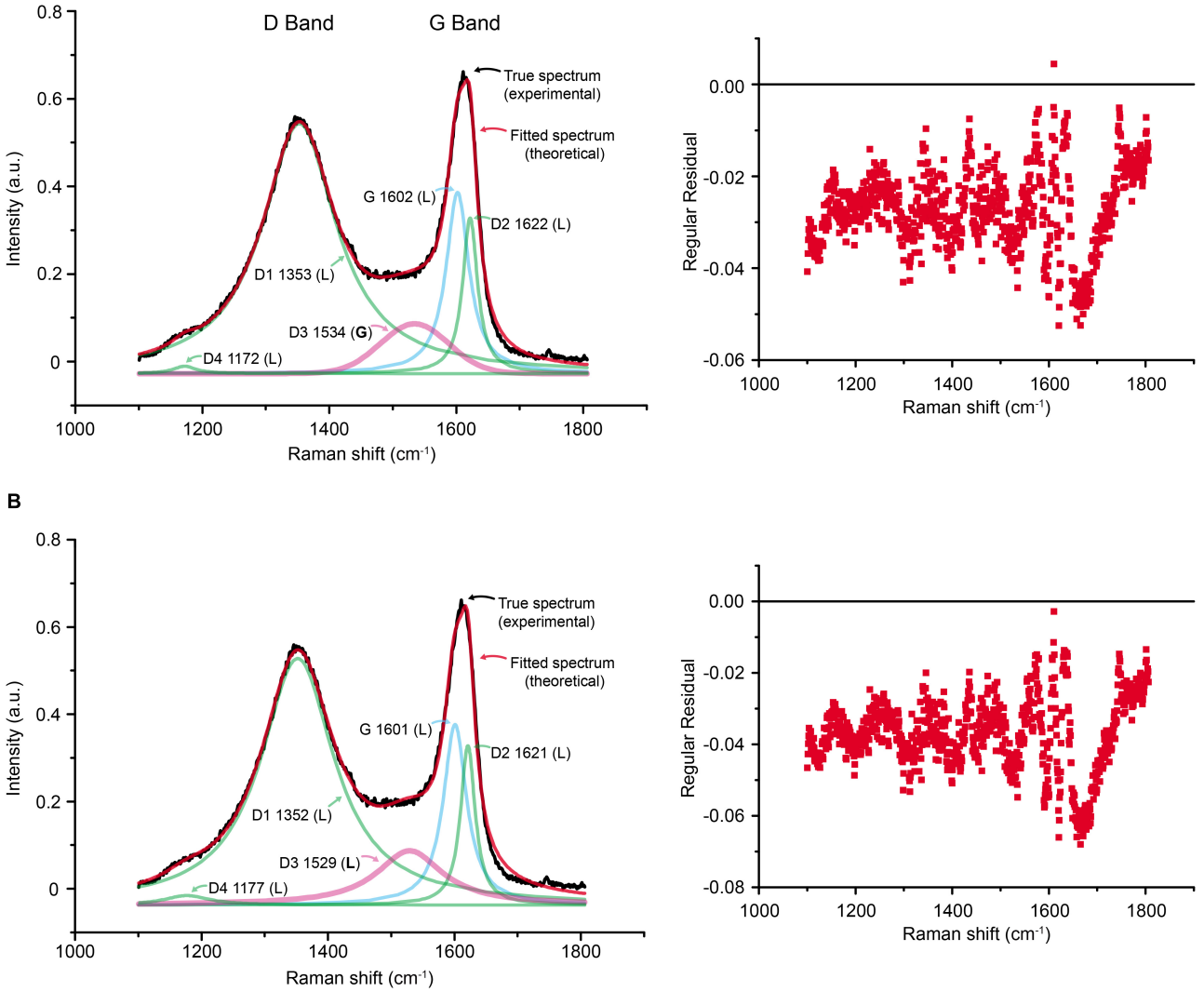

FIGURE 9 | Comparison of the two deconvolution methods. **(A)** The method of Sadezky et al. (2005) adopted in this study. **(B)** The method of Lahfid et al. (2010), which designated Lorentzian to D3 band (a pink curve). Note that overall regular residual is smaller in the first method. The numbers in each label of band are central position in the Raman shift; L and G in parenthesis denote Lorentzian and Gaussian distributions, respectively.

latirostris) does not show the one (**Figure 10E**) such as those figured in Marzola et al. (2015, Figures 9, 11). Thus, we could not investigate the reason behind the middle dark band of the modern crocodylian eggshells (**Table 3**) that should be further clarified by future studies.

TABLE 1 | Parameters of amorphous carbon peaks.

Deconvoluted bands	Band designation	Maximum height (a.u.)	Full width at half maximum (cm^{-1})	Area (a.u.)
G	Lorentzian	0.413	43.6	26.9
D1	Lorentzian	0.570	142	110
D2	Lorentzian	0.355	28.4	15.3
D3	Gaussian	0.114	126	15.2
D4	Lorentzian	0.0168	44.2	1.04

In summary, although similar in their position, the inner dark bands of *A. vesicularis* and extant *Caiman latirostris* (Crocodylia) eggshell have completely different backgrounds in their origin: dark bands of *A. vesicularis* is attributable to amorphous carbon (**Figures 8**, **9**), while those of (at least inner one) modern crocodylian eggshell would be caused by porous calcite (**Figure 10** and **Table 3**). It implies that the morphological or optical similarity alone should not be used as a diagnostic character before the reason behind the phenomenon is resolved by independent approach (e.g., Choi et al., 2020). For these reasons, despite crystallographic similarity, *A. vesicularis* cannot be safely ascribed to crocodyliform eggshell

TABLE 2 | Paleotemperature estimation based on Raman parameters.

T (°C) estimation formulae	Parametric values	Estimated paleotemperature (°C)
T = −445 X R2 + 641	[1]R2: 0.722	320
T = (RA1-0.3758)/0.0008	[2]RA1: 0.659	354
T = (RA2-0.27)/0.0045	[3]RA2: 1.93	369

[1]R2 = (D1 area)/(G area + D1 area + D2 area) (Beyssac et al., 2002). [2]RA1 = (D1 area + D4 area)/(G area + D1 area + D2 area + D3 area + D4 area) (Lahfid et al., 2010). [3]RA2 = (D1 area + D4 area)/(G area + D2 area + D3 area) (Lahfid et al., 2010).

before an organic-matter-derived dark band is reported from crocodyliform eggshell fossil.

With Fossil Eggshells

Gekkoolithus columnaris

Among the known fossil eggshells, *A. vesicularis* shows remarkable similarity with *Gekkoolithus columnaris* (Hirsch, 1996). Both ootaxa show a continuous dark band near the surface of the eggshell and have jagged columnar structure (**Figure 6**; Hirsch, 1996, Figure 4B). Unfortunately, Hirsch (1996) did not mention where the outer surface of the eggshell is in his Figure 4 thereby an accurate comparison when it comes to the location of the dark band is not possible. The average thickness of *A. vesicularis* (200 μm) is matched with an oogeneric diagnosis of *Gekkoolithus* (40–200 μm). Thus, the radial thin section images of both ootaxa have a significant degree of similarity.

Although Hirsch (1996) suggested the gekkotan affinity for *G. columnaris*, as admitted in his paper, the diagnosis of the *G. columnaris* was provisional and based on a morphological similarity with extant gekkotan eggshells. Recently, Choi et al. (2018) provided a more rigorous criterion to diagnose gekkotan eggshells in fossil record using the crystallographic configuration of eggshells (see also Choi et al., 2020). When the crystallography of *G. columnaris* is examined using EBSD and if it shows strong crystallographic similarity to modern gekkotan eggshells, *G. columnaris* can be concretely identified as a fossil squamate ootaxon. Otherwise (i.e., *G. columnaris* turns out to be an archosaur eggshell), the ootaxonomic affinity of *A. vesicularis* would be more strongly inclined to *G. columnaris*, and in this case, ironically, archosaurian '*Aenigmaoolithus*' might be synonymized with *Gekkoolithus* even though *Gekkoolithus* will not be a gekkotan ootaxon anymore.

Choristoderan Eggshell

The ornamentation of *A. vesicularis* is nodular with the flat top in radial view (**Figures 6H**, **7D–F**), similar to dispersituberculate ornamentation, which is reminiscent of choristoderan eggshell reported by Hou et al. (2009). See Potential egg-layer below for further discussion.

Maniraptoran Eggshells

Even though there have been many reports on eggshells with dispersituberculate ornamentation, these eggshells are usually thicker than 200 μm (Choi et al., 2020; Table 1) and many of them would be highly probable maniraptoran eggshells because at least two-layered crystallographic microstructure of maniraptoran dinosaur eggshells are observed (Choi et al., 2020) that is absent in *A. vesicularis* (**Figure 7**).

DISCUSSION

Dark Bands and Thermal Maturity

Dark Bands

It appears that fossil eggshells frequently preserve organic materials within the calcite. The presence of organic growth line in fossil eggshell has been frequently reported (see Grellet-Tinner et al., 2006; Jackson et al., 2010; Moreno-Azanza et al., 2014b for well-preserved growth lines). Those organic remnants may originate from structural proteins (e.g., Nys et al., 2004). Thermal alteration of these remnants may lead to form amorphous carbon. This interpretation can be further supported by the report that an antibody made from a chicken eggshell is also reactive to a sauropod eggshell, implying that the preserved organic matter in the sauropod eggshell is highly likely endogenous protein that survived more than 70 Myr (Schweitzer et al., 2005; but see also Saitta et al., 2018 for criticism). In addition, in some sub-fossil avian eggshells, easily degradable ancient DNA (aDNA) was preserved even from the warmer paleoenvironment suboptimal for aDNA preservation, meaning that the eggshell is effective in preserving fragile organic materials (Oskam et al., 2010; Demarchi et al., 2016; Grealy et al., 2017).

In this study, the presence of amorphous carbon in *A. vesicularis* was clearly observed (**Figure 8**). We see three potential hypotheses for the origin of the dark bands in *A. vesicularis*. Firstly, it may be the organic material of vertebrate preserved *in situ* as in Schweitzer et al. (2005). The systematic (linear) distribution of carbonaceous matter (**Figure 8D**), which is reminiscent of that of modern avian eggshell (e.g., Fraser et al., 1998) supports this view. Secondly, the carbonaceous materials may be mainly derived from the microbial activity after the egg was buried in earth. In this case, although potential *in situ* original distribution of carbonaceous matter may cause the pattern seen in **Figure 8** (as in first hypothesis), because the proteins would be a main target of microbe, the detected carbonaceous matter may be mainly derived from microbe, not from the endogenous protein of the eggshell. The second hypothesis can be supported by the omnipresence of microbe in the crust of earth (even if *A. vesicularis* experienced heat effect and deep burial; Edwards et al., 2007; Magnabosco et al., 2018), the ancient and relatively modern microbial activity in the fossil materials (Kremer et al., 2012; Owocki et al., 2016; Saitta et al., 2019b), and experimental evidences (Smith and Hayward, 2010). Thirdly, the carbonaceous material may be derived from inorganic carbonaceous material. We think that the third hypothesis is less likely considering the scarcity of amorphous carbon signal in the surrounding matrix (**Figure 8D**).

Despite the aforementioned utility, we note that Raman spectroscopy alone does not provide full details of the origin of carbonaceous matters preserved in geological materials (i.e., biogenic or not) (Pasteris and Wopenka, 2003; Marshall et al., 2010). Other analytical techniques may reveal whether

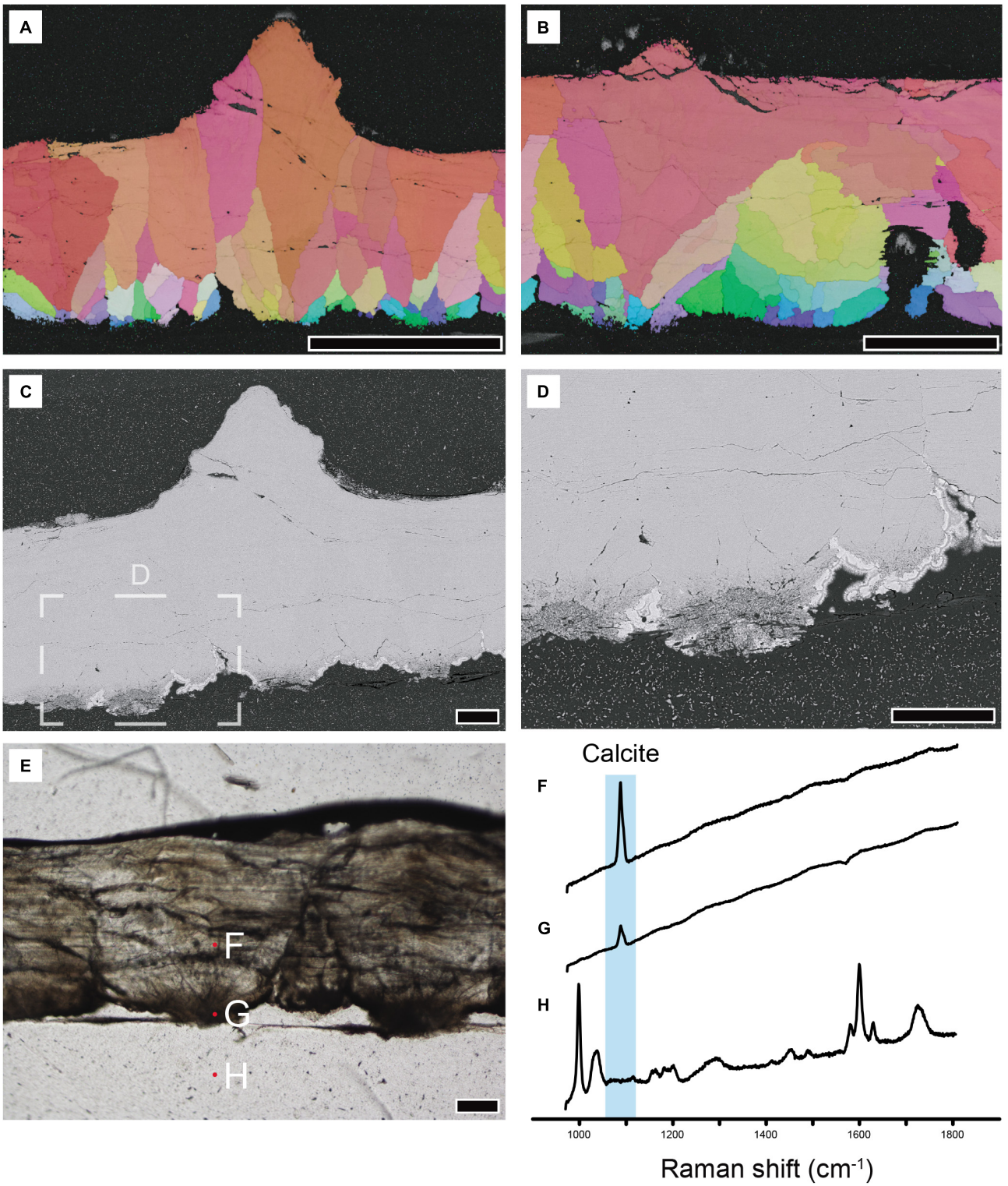

FIGURE 10 | Modern crocodylian (*Caiman latirostris*; UHR33185) eggshell analyzed with selected methods. **(A,B)** IPF maps. Note wedge-like calcite grains of crocodylian eggshell. Grains with horizontal *c*-axis is present toward the middle of the eggshell. **(C,D)** BSE imaging. Note that the inner end of the eggshell is composed of porous calcite. **(E)** Thin section imaging and locations where Raman spectra were acquired. Note that the inner dark band corresponds to the porous calcite figured in **(D)** above. **(F–H)** Raman spectra acquired at the locations marked in **(E)**. **(F,G)** In plain calcite and a dark part at the inner end of the eggshell, only calcite Raman peak is detected. Note the absence of amorphous carbon peaks (i.e., G,D bands) in **(G)**. **(H)** A spectrum from epoxy resin shows the peaks attributable to polyester resin and silica gel. Scale bars equal 500 μm **(A)**; 250 μm **(B)**; 100 μm **(C–E)**.

TABLE 3 | Comparison between the dark bands of *Caiman latirostris* (crocodyliformes) eggshell and *A. vesicularis*.

	Position	Width portion	Width (μm)	Origin
Caiman latirostris	Inner end	9.97%	47.3	Porosity of calcite
A. vesicularis	Inner end and middle part	25.16% (inner); 19.89% (middle)	59.5 (inner); 47.0 (middle)	Amorphous carbon

the carbonaceous material is biogenic or not (see Figure 4 of Pasteris and Wopenka, 2003). For example, these techniques include Gas-Chromatography/Mass-Spectrometry (Gupta et al., 2007; Saitta et al., 2019b) and/or stable isotope analysis concentrated on the $\delta^{13}C$ value (Schidlowski, 2001; Bell et al., 2015). Because the available specimen of *A. vesicularis* was not sufficient, currently, it is impossible to try further independent analysis with this sample.

Taking the distribution of amorphous carbon into consideration (**Figure 8**), the precursor of amorphous carbon in *A. vesicularis* would be most likely from intercrystalline protein (Schweitzer et al., 2005) and its biogenic contamination derived from Late Cretaceous or relatively modern (but geologic past such as Cenozoic) microbes (Kremer et al., 2012; Saitta et al., 2019b). If the latter is the case, the thermal estimation (**Table 2**) should not be used as Late Cretaceous paleotemperatural state of the Daeri Andesite. Nevertheless, it would still show the taphonomic history that *A. vesicularis* experienced. Extant microbes (e.g., Saitta et al., 2019b) would not be source of the dark band because what we detected is thermally matured carbonaceous matter, not pristine organic matter.

Thermal Maturity

The presence of carbonaceous matter (in our case, the dark bands) in the fossil materials can be used in estimating the thermal maturity of the fossil through Raman spectroscopy (see section "Introduction" above). The amorphous carbon in the dark band of *A. vesicularis* shows characteristic G and D bands in the Raman spectrum (**Figures 8**, **9**). In pure graphite, only G band exists (Tuinstra and Koenig, 1970), but the intense heat effect disrupts the structure, causing D band (Ferrari and Robertson, 2000). Numerous studies have shown that the peak shape and the relative intensities of G and D bands depend on thermal maturity of preserved carbonaceous matter (e.g., Schopf et al., 2005; Schiffbauer et al., 2012; Hartkopf-Fröder et al., 2015; McNeil et al., 2015; Olcott Marshall and Marshall, 2015; Schito et al., 2017; Henry et al., 2019a,b). The spectral information, therefore, can be used for reconstructing the thermal history of the fossil materials (Schopf et al., 2005).

Aenigmaoolithus vesicularis shows G and D bands and yields Raman parameters (**Table 1**) that may provide the opportunity to systematically (and quantitatively) compare the carbonaceous thermal maturity among the spatiotemporally diverse fossil eggshell materials around the globe (especially where near the convergent margin of plates). Korean fossil eggshell materials would be ideal ones to investigate the thermal effect on the carbonaceous matter because Cretaceous deposits in the Korean Peninsula were heavily influenced by volcanic activity and magmatism during the Cretaceous and Paleogene (Chough and Sohn, 2010; Zhang et al., 2012; Kim S.W. et al., 2016; Zhai et al., 2016; Kwon et al., 2017; Hwang et al., 2019). Wi Island is not an exception and it is also highly influenced by the Late Cretaceous volcanism (Gihm and Hwang, 2014; Gihm et al., 2017; Ko et al., 2017). However, most studies did not pay attention to the extent of heat effect, but just mentioned the presence of it. In other words, the quantitative approaches have been uncommon. Thus, the approach attempted in this study may provide a way to estimate the thermal history of terrestrial basin using macrofossil (= fossil egg).

The thermally matured organic matter (i.e., blackened amorphous carbon) would be, at least partially, responsible for usual dark-color of Korean fossil eggshells (e.g., Janssen et al., 2011; Collins and Steele, 2017) along with blackening chamosite, a mineral that is widespread in Korean Cretaceous vertebrate bones and invertebrate shells (Kim et al., 2018; **Supplementary Figure S4**). In fact, palynomorphs from the Cretaceous deposits in Korea are heavily altered by igneous activities as well (Choi, 1985, 1989; Yi et al., 1998, 2004), supporting that thermal maturation of the carbonaceous material was a universal phenomenon for Cretaceous fossils in the Korean Peninsula.

We suggest that comparing the Raman spectra of fossil eggshells (or any other type of fossil that preserve carbonaceous matter) from where Cretaceous volcanism and magmatism were intense (e.g., northeastern and southern China, Korea, and Japan; Chough and Sohn, 2010; Pan et al., 2013; Song et al., 2015; Zhai et al., 2016; Ryu and Lee, 2017) to those from relatively stable regions (e.g., inland China and Mongolia; Eberth et al., 2009; Zhang et al., 2014; Eberth, 2018) in East Asia would make it possible to assess the potential relationship between the thermal maturity of fossils and the tectonic setting in a more systematic way (see also Choi and Lee, 2011 and Song et al., 2015 for the thermal history of northeastern China, Korea, and Japan where are relevant to the continental margin tectonism).

Although it is not presented herein, we observed well-developed amorphous carbon peaks from the *Reticuloolithus acicularis*, sympatric to *A. vesicularis* (Choi and Lee, 2019). The accuracy of the estimated paleotemperature would be a potential future research avenue because thermal maturity assessment has been mostly focused on the marine microfossil (see section "Introduction" above), but to our knowledge, few study has focused on thermal maturity of terrestrial macrofossil. A systematic taphonomic experiment that controls temperature and/or pressure would be also helpful for such an approach (e.g., Saitta et al., 2019a).

Finally, we note that the amorphous carbon signal of *A. vesicularis* is not the first report of amorphous carbon from fossil eggshells. Stein et al. (2019, Supplementary Figure S2) recently reported that the Raman spectroscopy detected the presence of amorphous carbon peaks (i.e., G and D bands) from the eggshell of *Massospondylus* from the Lower Jurassic Elliot Formation of South Africa. However, Stein et al. (2019) interpreted the signal as an artifact due to laser ablation triggered by the long exposure time of Raman analysis. We would not like to negate such a possibility because the laser powers used in Stein et al. (2019) (2.5–25 mW) and this study were not

controlled (∼11 mA) and the preservation of carbonaceous matter of both fossil specimens might have affected the volatility when exposed to laser. Nevertheless, 2D Raman mapping (e.g., **Figure 8**) will make it possible to test whether the signal in Stein et al. (2019, Supplementary Figure S2) is indeed an artifact or is a part of the potential biogenic structure of the eggshell. Although further investigation is necessary, the observed amorphous carbon in *Massospondylus* eggshell may originate from organic materials inside an eggshell (and/or its accompanying microbiome), providing potential insight into the thermal evolution of the Elliot Formation (e.g., Schopf et al., 2005; McNeil et al., 2015; this study).

Potential Egg-Layer

The egg layer of *A. vesicularis* is enigmatic because there is no significantly similar egg fossil in the literature except for an affinity unknown ootaxon *Gekkoolithus* (Hirsch, 1996). Nevertheless, the available evidence confines it to unequivocal archosaur affinity (see EBSD observation above). We propose that non-dinosaur archosaurs such as Crocodyliformes or Choristodera may be a potential egg layer. Considering the small size of egg, extreme thinness, and peculiar microstructure of *A. vesicularis* that is dissimilar to those of eggshell of Maniraptora (Choi et al., 2020) which is the only known dinosaur clade that laid small (comparable to the estimated size of *A. vesicularis*) eggs, it is unlikely that *A. vesularis* is a dinosaur egg.

As discussed above, the crocodyliform affinity cannot be ruled out. However, we would not support the crocodyliform affinity until the middle dark band of fossil and modern crocodyliform eggshell turns out to have an organic origin.

Although detailed direct evidence should be gathered, we speculate (or hypothesize) that another potential egg-layer may be Choristodera. Firstly, Choristodera was one of the major clades of paleoecosystem in the Early Cretaceous of East Asia. The reported choristoderan genera outnumber that of crocodyliforms at that time only in Asia (Matsumoto and Evans, 2010, Figure 5). Interestingly, Choristodera was reported from the Lower Cretaceous deposits of China and Japan (Matsumoto and Evans, 2010, Table 4), thereby it is highly probable that they also existed in the Early Cretaceous of Korea considering that China, Korea, and Japan were connected landmasses before Miocene (Taira, 2001; Chough and Sohn, 2010; Van Horne et al., 2017). Admittedly, the record of Choristodera from the Upper Cretaceous deposits in Asia is nearly absent (Matsumoto et al., 2019a), but a preliminary report of Choristodera from the Upper Cretaceous deposits (Kuji Group) of northeast Japan implies that the lack of record may be attributable to the taphonomic bias (Matsumoto et al., 2019b). Secondly, the surface ornamentation composed of the circular flat-topped node was reported in *Hyphalosaurus baitaigouensis* (Choristodera) eggshell (Hou et al., 2009). This structure is similar to that of Korean specimen in this study (**Figures 6H**, **7D–F**). If both structures are homologous to each other (i.e., not an outcome of independent homoplastic evolution), this character can be used to support the choristoderan affinity of *A. vesicularis* among the non-dinosaur archosaurs because there is no report of flat-topped nodular ornamentation in extant and fossil crocodyliform eggshells.

However, 'choristoderan affinity' hypothesis is not without weakness. All known Choristodera laid soft eggshells unlike *A. vesicularis* (Ji et al., 2006; Hou et al., 2009) or are suggested to be viviparous (Ji et al., 2010; Blackburn and Sidor, 2014). There is no report of rigid eggshells in Choristodera so far (Sander, 2012; Skawiñski and Tałanda, 2014). However, Stein et al. (2019) opened a discussion that well-mineralized rigid eggshells might have been independently evolved from very thin calcified eggshells in different dinosaur clades. In addition, a crystallographic approach for the rigid and soft eggshells of Gekkota showed a similar framework in their configuration, despite difference in their degree of mineralization, having a homologous blueprint in their eggshells (Choi et al., 2018). These cases demonstrate that the rigid eggshell can be readily evolved from the soft eggshell that can be further supported by the independent evolution of rigid eggshells in non-gekkotan squamates (i.e., Early Cretaceous anguimorph eggshells; Fernandez et al., 2015).

That being said, this hypothesis should be tested. When the crystallography of an authentic choristoderan eggshell (e.g., Ji et al., 2006; Hou et al., 2009) is analyzed and compared with *A. vesicularis*, the 'choristoderan affinity' hypothesis of *A. vesicularis* can be solved with firm data. More importantly, the correct identification of Choristodera eggshell through crystallographic approach (e.g., Choi et al., 2020) would help to clarify exact taxonomic status of Choristodera. That is because choristoderan eggshell affinity to either archosaur- or lepidosaurian-type eggshell through crystallographic approach (e.g., Choi et al., 2020) will provide an indirect evidence to the true affinity (either archosaur or lepidosaurian) of choristodera that is still a controversial issue in vertebrate paleontology (see Matsumoto and Evans, 2010, p. 254).

In summary, *A. vesicularis* is most comparable to the crocodyliform eggshell among the known well-studied archosaur eggshells. Nevertheless, considering the very conservative nature of crocodyliform eggshells (or basal archosaur in general) (Moreno-Azanza et al., 2015), observed common characters in crocodilyform eggshell and *A. vesicularis* may not be unique to crocodyliform eggshells but may be present in other primitive archosaur eggshells (e.g., Choristodera or other non-crocodyliform basal Crurotarsi).

CONCLUSION

An enigmatic fossil egg from the Wido Volcanics of South Korea named as *Aenigmaoolithus vesicularis* has typical archosaurian microstructure and crystallography. We confirmed that dark bands in *A. vesicularis* are carbon in origin by detecting the G and D bands from the Raman spectrum. The presence of amorphous carbon in the eggshell can be used in quantitative way when assessing the thermal maturity of fossil materials. This approach would be applicable to other regions in East Asia which were also affected by Cretaceous igneous activity. It will be also useful to screen out thermally altered fossil materials before performing molecular paleontological investigation, which is aimed for finding

pristine molecular traces in the fossil record (e.g., Oskam et al., 2011). Finally, the taxonomic affinity of *A. vesicularis* is unknown, but we propose that non-dinosaur archosaur such as Crocodyliformes or Choristodera may be the potential candidates based on crystallography, ornamentation morphology, paleobiogeography, and potential independent origin of eggshell mineralization. We suggest future research should be done for the crystallography of genuine choristoderan eggshells to test the true affinity of *A. vesicularis*. This approach will also provide an independent evidence to resolve the controversial phylogenetic position of Choristodera.

DATA AVAILABILITY STATEMENT

The datasets generated for this study are available on request to the corresponding author.

AUTHOR CONTRIBUTIONS

SC and Y-NL designed the research with inputs from SL. SC, N-HK, SK, and Y-NL did fieldwork. SC and SL conducted analyses and collected data. SC and N-HK wrote the original manuscript and prepared figures except for those of geological setting, which were done by SK. All authors reviewed and edited the manuscript.

FUNDING

This research was supported by the National Research Foundation of Korea (grant number: 2019R1A2B5B020 70240) to Y-NL. SL was supported by the National Research Foundation of Korea (grant number: 2017R1A2A1A17069511).

ACKNOWLEDGMENTS

Kohei Tanaka (University of Tsukuba) and Hiroki Echizenya (Hokkaido University Museum) generously provided modern crocodylian eggshells to SC. Tzu-Ruei Yang (National Museum of Natural Science, Taiwan) suggested an idea of using Raman spectroscopy to SC that was adopted in this study. Taehyun Kim and Yongjae Lee (Yonsei University) kindly provided their unpublished data (**Supplementary Figure S4**). Hyo-Im Kim and Yong-Hyun Kim (SEES, SNU) helped SC and SL in Raman spectroscopic analysis, Jihyuk Kim and Seokyoung Han (SEES, SNU) provided their polarized light microscope. Jin Kang and Seolji Kim (NCIRF, SNU) helped SC in using Raman spectrometer and FE-EPMA, respectively. SC thanks Duck Keun Choi (SEES, SNU) for discussion. We thank the reviewers GP (Universidad de la República de Uruguay), AO (University of Kansas), and associate editor PS (University of Kansas) who greatly improved the quality of the manuscript.

SUPPLEMENTARY MATERIAL

The Supplementary Material for this article can be found online at: https://www.frontiersin.org/articles/10.3389/feart.2019.00349/full#supplementary-material

REFERENCES

Angst, D., Amiot, R., Buffetaut, E., Fourel, F., Martineau, F., Lazzerini, N., et al. (2015). Diet and climatic context of giant birds inferred from $\delta^{13}C_c$ and $\delta^{18}O_c$ values of Late Palaeocene and Early Eocene eggshells from southern France. *Palaeogeogr. Palaeoclimatol. Palaeoecol.* 435, 210–221. doi: 10.1016/j.palaeo.2015.06.011

Ar, A., Rahn, H., and Paganelli, C. V. (1979). The avian egg: mass and strength. *Condor* 81, 331–337. doi: 10.2307/1366955

Athanasiadou, D., Jiang, W., Goldbaum, D., Saleem, A., Basu, K., Pacella, M. S., et al. (2018). Nanostructure, osteopontin, and mechanical properties of calcitic avian eggshell. *Sci. Adv.* 4:eaar3219. doi: 10.1126/sciadv.aar3219

Bell, E. A., Boehnke, P., Harrison, T. M., and Mao, W. L. (2015). Potentially biogenic carbon preserved in a 4.1 billion-year-old zircon. *Proc. Natl. Acad. Sci. U.S.A.* 112, 14518–14521. doi: 10.1073/pnas.1517557112

Bernard, S., Benzerara, K., Beyssac, O., Menguy, N., Guyot, F., Brown, G. E. Jr., et al. (2007). Exceptional preservation of fossil plant spores in high-pressure metamorphic rocks. *Earth Planet. Sci. Lett.* 262, 257–272. doi: 10.1016/j.epsl.2007.07.041

Beyssac, O., Goffé, B., Chopin, C., and Rouzaud, J. N. (2002). Raman spectra of carbonaceous material in metasediments: a new geothermometer. *J. Metamorp. Geol.* 20, 859–871. doi: 10.1046/j.1525-1314.2002.00408.x

Blackburn, D. G., and Sidor, C. A. (2014). Evolution of viviparous reproduction in Paleozoic and mesozoic reptiles. *Int. J. Dev. Biol.* 58, 935–948. doi: 10.1387/ijdb.150087db

Casella, L. A., Griesshaber, E., Simonet Roda, M., Ziegler, A., Mavromatis, V., Henkel, D., et al. (2018). Micro- and nanostructures reflect the degree of diagenetic alteration in modern and fossil brachiopod shell calcite: a multi-analytical screening approach (CL, FE-SEM, AFM, EBSD). *Palaeogeogr. Palaeoclimatol. Palaeoecol.* 502, 13–30. doi: 10.1016/j.dib.2018.05.041

Choi, D. K. (1985). Spores and pollen from the Gyeongsang Supergroup, southeastern Korea and their chronologic and paleoecologic implications. *J. Paleontol. Soc. Korea* 1, 33–50.

Choi, D. K. (1989). Paleopalynology of the Geoncheonri Formation (Lower Cretaceous), Geoncheon-Ahwa area, Korea. *J. Paleontol. Soc. Korea* 5, 1–27.

Choi, S., and Lee, Y.-N. (2017). A review of vertebrae body fossils from the Korean Peninsula and perspectives. *Geosci. J.* 21, 867–889. doi: 10.1007/s12303-017-0040-6

Choi, S., and Lee, Y.-N. (2019). Possible Late Cretaceous dromaeosaurid eggshells from South Korea: a new insight into dromaeosaurid oology. *Cretac. Res.* 103:104167. doi: 10.1016/j.cretres.2019.06.013

Choi, S., Han, S., and Lee, Y.-N. (2019). Electron backscatter diffraction (EBSD) analysis of maniraptoran eggshells with important implications for microstructural and taphonomic interpretations. *Palaeontology* 62, 777–803. doi: 10.1111/pala.12427

Choi, S., Han, S., Kim, N.-H., and Lee, Y.-N. (2018). A comparative study of eggshells of Gekkota with morphological, chemical compositional and crystallographic approaches and its evolutionary implications. *PLoS One* 13:e0199496. doi: 10.1371/journal.pone.0199496

Choi, S., Moreno-Azanza, M., Csiki-Sava, Z., Prondvai, E., and Lee, Y.-N. (2020). Comparative crystallography suggests maniraptoran theropod affinities for latest Cretaceous European 'geckoid' eggshells. *Pap. Palaeontol.* doi: 10.1002/spp2.1294

Choi, T., and Lee, Y. I. (2011). Thermal histories of Cretaceous basins in Korea: implications for response of the East Asian continental margin to subduction of the Paleo-Pacific Plate. *Isl. Arc.* 20, 371–385. doi: 10.1111/j.1440-1738.2011.00771.x

Chough, S. K., and Sohn, Y. K. (2010). Tectonic and sedimentary evolution of a Cretaceous continental arc-backarc system in the Korean peninsula: new view. *Earth-Sci. Rev.* 101, 225–249. doi: 10.1016/j.earscirev.2010.05.004

Chough, S. K., Kwon, S.-T., Ree, J.-H., and Choi, D. K. (2000). Tectonic and sedimentary evolution of the Korean peninsula: a review and new view. *Earth-Sci. Rev.* 52, 175–235. doi: 10.1016/s0012-8252(00)00029-5

Collins, B., and Steele, T. E. (2017). An often overlooked resource: ostrich (*Struthio* spp.) eggshell in the archaeological record. *J. Archaeol. Sci. Rep.* 13, 121–131. doi: 10.1016/j.jasrep.2017.03.036

Cusack, M., and Freer, A. (2008). Biomineralization: elemental and organic influence in carbonate systems. *Chem. Rev.* 108, 4433–4454. doi: 10.1021/cr078270o

Dauphin, Y., Luquet, G., Perez-Huerta, A., and Salomé, M. (2018). Biomineralization in modern avian calcified eggshells: similarity versus diversity. *Connect. Tissue Res.* 58, 67–73. doi: 10.1080/03008207.2018.1430144

Demarchi, B., Hall, S., Roncal-Herrero, T., Freeman, C. L., Woolley, J., Crisp, M. K., et al. (2016). Protein sequences bound to mineral surfaces persist into deep time. *eLife* 5:e17092. doi: 10.7554/eLife.17092

Eberth, D. A. (2018). Stratigraphy and paleoenvironmental evolution of the dinosaur-rich Baruungoyot-Nemegt succession (Upper Cretaceous), Nemegt Basin, southern Mongolia. *Palaeogeogr. Palaeoclimatol. Palaeoecol.* 494, 29–50. doi: 10.1016/j.palaeo.2017.11.018

Eberth, D. A., Kobayashi, Y., Lee, Y.-N., Mateus, O., Therrien, F., Zelenitsky, D. K., et al. (2009). Assignment of *Yamaceratops dorngobiensis* and associated redbeds at Shine Us Khudag (Eastern Gobi, Dorngobi Province, Mongolia) to the redescribed Javkhlant Formation (Upper Cretaceous). *J. Vert. Paleontol.* 29, 295–302. doi: 10.1080/02724634.2009.10010384

Edwards, H. G. M., Jorge Villar, S. E., Pullan, D., Hargreaves, M. D., Hofmann, B. A., and Westall, F. (2007). Morphological biosignatures from relict fossilised sedimentary geological specimens: a Raman spectroscopic study. *J. Raman Spectrosc.* 38, 1352–1361. doi: 10.1002/jrs.1775

Ferguson, M. W. J. (1982). The structure and composition of the eggshell and embryonic membranes of *Alligator mississippiensis*. *Trans. Zool. Soc. Lond.* 36, 99–152. doi: 10.1111/j.1096-3642.1982.tb00064.x

Fernández, M. S., Simoncini, M. S., and Dyke, G. (2013). Irregularly calcified eggs and eggshells of *Caiman latirostris* (Alligatoridae: Crocodylia). *Naturwissenschaften* 100, 451–457. doi: 10.1007/s00114-013-1044-3

Fernandez, V., Buffetaut, E., Suteethorn, V., Rage, J.-C., Tafforeau, P., and Kundrát, M. (2015). Evidence of egg diversity in squamate evolution from Cretaceous anguimorph embryos. *PLoS One* 10:e0128610. doi: 10.1371/journal.pone.0128610

Ferralis, N., Matys, E. D., Knoll, A. H., Hallmann, C., and Summons, R. E. (2016). Rapid, direct and non-destructive assessment of fossil organic matter via micro Raman spectroscopy. *Carbon* 108, 440–449. doi: 10.1016/j.carbon.2016.07.039

Ferrari, A. C., and Robertson, J. (2000). Interpretation of Raman spectra of disordered and amorphous carbon. *Phys. Rev. B* 61, 14095–14107. doi: 10.1103/physrevb.61.14095

Fraser, A. C., Bain, M. M., and Solomon, S. E. (1998). Organic matrix morphology and distribution in the palisade layer of eggshells sampled at selected periods during lay. *Br. Poult. Sci.* 39, 225–228. doi: 10.1080/00071669889169

Gihm, Y. S., and Hwang, I. G. (2014). Syneruptive and intereruptive lithofacies in lacustrine environments: the Cretaceous Beolkeum Member, Wido Island, Korea. *J. Volcanol. Geotherm. Res.* 273, 15–32. doi: 10.1016/j.jvolgeores.2014.01.004

Gihm, Y. S., and Hwang, I. G. (2016). Lacustrine hyperpycnal flow deposits after explosive volcanic eruptions, Cretaceous Beolkeum Member, Wido Island, Korea. *Geosci. J.* 20, 157–166. doi: 10.1007/s12303-015-0040-3

Gihm, Y. S., Kim, M.-C., Son, M., and Hwang, I. G. (2017). The influence of tectonic subsidence on volcaniclastic sedimentation: the Cretaceous upper Daeri Member, Wido Island, Korea. *Isl. Arc* 26:e12183. doi: 10.1111/iar.12183

Graf, J., Tabor, N. J., Ferguson, K., Winkler, D. A., Lee, Y.-N., May, S., et al. (2018). Diagenesis of dinosaur eggshell from the Gobi Desert, Mongolia. *Palaeogeogr. Palaeoclimatol. Palaeoecol.* 494, 65–74. doi: 10.1016/j.palaeo.2017.11.011

Grealy, A., Phillips, M., Miller, G., Gilbert, M. T. P., Rouillard, J.-M., Lambert, D., et al. (2017). Eggshell palaeogenomics: palaeognath evolutionary history revealed through ancient nuclear and mitochondrial DNA from Madagascan elephant bird (*Aepyornis* sp.) eggshell. *Mol. Phylogenet. Evol.* 109, 151–163. doi: 10.1016/j.ympev.2017.01.005

Grellet-Tinner, G. (2005). Membrana testacea of titanosaurid dinosaur eggs from Auca Mahuevo (Argentina): implications for exceptional preservation of soft tissue in Lagerstätten. *J. Vert. Paleontol.* 25, 99–106. doi: 10.1671/0272-4634(2005)025%5B0099:mtotde%5D2.0.co;2

Grellet-Tinner, G., Chiappe, L., Norell, M., and Bottjer, D. (2006). Dinosaur eggs and nesting behaviors: a paleobiological investigation. *Palaeogeogr. Palaeoclimatol. Palaeoecol.* 232, 294–321. doi: 10.1016/j.palaeo.2005.10.029

Grellet-Tinner, G., Corsetti, F., and Buscalioni, A. D. (2010). The importance of microscopic examinations of eggshells: discrimination of bioalteration and diagenetic overprints from biological features. *J. Iber. Geol.* 36, 181–192. doi: 10.5209/rev_jige.2010.v36.n2.6

Grigorescu, D. (2017). The 'Tuştea puzzle' revisited: Late Cretaceous (Maastrichtian) *Megaloolithus* eggs associated with *Telmatosaurus* hatchlings in the Haţeg Basin. *Hist. Biol.* 29, 627–640. doi: 10.1080/08912963.2016.1227327

Gupta, N. S., Tetlie, O. E., Briggs, D. E. G., and Pancost, R. D. (2007). The fossilization of euryapterids: a result of molecular transformation. *Palaios* 22, 439–447. doi: 10.2110/palo.2006.p06-057r

Hartkopf-Fröder, C., Königshof, P., Littke, R., and Schwarzbauer, J. (2015). Optical thermal maturity parameters and organic geochemical alteration at low grade diagenesis to anchimetamorphism: a review. *Int. J. Coal Geol.* 150–151, 74–119. doi: 10.1016/j.coal.2015.06.005

Henry, D. G., Jarvis, I., Gillmore, G., and Stephenson, M. (2019a). A rapid method for determining organic matter maturity using Raman spectroscopy: application to Carboniferous organic-rich mudstones and coals. *Int. J. Coal Geol.* 203, 87–98. doi: 10.1016/j.coal.2019.01.003

Henry, D. G., Jarvis, I., Gillmore, G., and Stephenson, M. (2019b). Raman spectroscopy as a tool to determine the thermal maturity of organic matter: Application to sedimentary, metamorphic and structural geology. *Earth-Sci. Rev.* 198:102936. doi: 10.1016/j.earscirev.2019.102936

Hincke, M. T., Nys, Y., Gautron, J., Mann, K., Rodriguez-Navarro, A. B., and McKee, M. D. (2012). The eggshell: structure, composition and mineralization. *Front. Biosci.* 17, 1266–1280. doi: 10.2741/3985

Hirsch, K. F. (1996). Parataxonomic classification of fossil chelonian and gecko eggs. *J. Vert. Paleontol.* 16, 752–762. doi: 10.1080/02724634.1996.10011363

Hirsch, K. F., and Quinn, B. (1990). Eggs and eggshell fragments from the Upper Cretaceous Two Medicine Formation of Montana. *J. Vert. Paleontol.* 10, 491–511. doi: 10.1080/02724634.1990.10011832

Hou, L.-H., Li, P.-P., Ksepka, D. T., Gao, K.-Q., and Norell, M. A. (2009). Implications of flexible-shelled eggs in a Cretaceous choristoderan reptile. *Proc. R. Soc. B* 277, 1235–1239. doi: 10.1098/rspb.2009.2035

Hwang, S. K., Kim, S. W., Kee, W.-S., and Kim, J. J. (2019). U-Pb zircon ages and division of the Cretaceous volcanic arc in the Korean Peninsula: spatiotemporal evolution of the arc volcanism. *J. Geol. Soc. Korea* 55, 595–619. (in Korean with English abstract). doi: 10.14770/jgsk.2019.55.5.595

Jackson, F. D., and Varricchio, D. J. (2016). Fossil egg and eggshells from the Upper Cretaceous Hell Creek Formation, Montana. *J. Vert. Paleontol.* 36:e1185432. doi: 10.1080/02724634.2016.1185432

Jackson, F. D., Horner, J. R., and Varricchio, D. J. (2010). A study of a *Troodon* egg containing embryonic remains using epifluorescence microscopy and other techniques. *Cretac. Res.* 31, 255–262. doi: 10.1016/j.cretres.2009.11.006

Janssen, J. D., Mutch, G. W., and Hayward, J. L. (2011). Taphonomic effects of high temperature on avian eggshell. *Palaios* 26, 658–664. doi: 10.2110/palo.2011.p11-012r

Ji, Q., Ji, S.-A., Lü, J., You, H., and Yuan, C.-X. (2006). Embryos of Early Cretaceous Choristodera (Reptilia) from the Jehol biota in Western Liaoning, China. *J. Paleontol. Soc. Korea* 22, 111–118.

Ji, Q., Wu, X.-C., and Cheng, Y.-N. (2010). Cretaceous choristoderan reptiles gave birth to live young. *Naturwissenschaften* 97, 423–428. doi: 10.1007/s00114-010-0654-2

Khatibi, S., Ostadhassan, M., Hackley, P., Tuschel, D., Abarghani, A., and Bubach, B. (2019). Understanding organic matter heterogeneity and maturation rate by

Raman spectroscopy. *Int. J. Coal Geol.* 206, 46–64. doi: 10.1016/j.coal.2019.03.009

Kim, E. J., Fei, Y., and Lee, S. K. (2016). Probing carbon-bearing species and CO_2 inclusions in amorphous carbon-$MgSiO_3$ enstatite reaction products at 1.5 GPa: insights from ^{13}C high-resolution solid-state NMR. *Am. Mineral.* 101, 1113–1124. doi: 10.2138/am-2016-5563

Kim, N. H., Choi, S., Kim, S., and Lee, Y.-N. (2019). A new faveoloolithid oogenus from the Wido Volcanics (Upper Cretaceous), South Korea and a new insight into the oofamily Faveoloolithidae. *Cretac. Res.* 100, 145–163. doi: 10.1016/j.cretres.2019.04.001

Kim, S. W., Kwon, S., Park, S.-I., Lee, C., Cho, D.-L., Lee, H.-J., et al. (2016). SHRIMP U-Pb dating and geochemistry of the Cretaceous plutonic rocks in the Korean Peninsula: a new tectonic model of the Cretaceous Koran Peninsula. *Lithos* 262, 88–106. doi: 10.1016/j.lithos.2016.06.027

Kim, T., Lee, Y., and Lee, Y.-N. (2018). Fluorapatite diagenetic differences between Cretaceous skeletal fossils of Mongolia and Korea. *Palaeogeogr. Palaeoclimatol. Palaeoecol.* 490, 579–589. doi: 10.1016/j.palaeo.2017.11.047

Ko, K., Kim, S. W., Lee, H.-J., Hwang, I. G., Kim, B. C., Kee, W.-S., et al. (2017). Soft sediment deformation structures in a lacustrine sedimentary succession induced by volcano-tectonic activities: an example from the Cretaceous Beolgeumri Formation, Wido Volcanics, Korea. *Sediment. Geol.* 358, 197–209. doi: 10.1016/j.sedgeo.2017.07.008

Koh, H. J., Kwon, C. W., Park, S. I., Park, J., and Kee, W.-S. (2013). *Geological Report of the Julpo and Wido Hawangdeungdo Sheets (1:50000)*. Daejeon: Korea Institute of Geoscience and Mineral Resources. (in Korean with English abstract).

Kohring, R. R. (1999). Calcified shell membranes in fossil vertebrate eggshell: evidence for preburial diagenesis. *J. Vert. Paleontol.* 19, 723–727. doi: 10.1080/02724634.1999.10011184

Kohring, R., and Hirsch, K. F. (1996). Crocodilian and avian eggshells from the Middle Eocene of the Geiseltal, Eastern Germany. *J. Vert. Paleontol.* 16, 67–80. doi: 10.1080/02724634.1996.10011285

Kraus, M. J. (1999). Paleosols in clastic sedimentary rocks: their geological applications. *Earth-Sci. Rev.* 47, 41–70. doi: 10.1016/s0012-8252(99)00026-4

Kremer, B., Owocki, K., Królikowska, A., Wrzosek, B., and Kazmierczak, J. (2012). Mineral microbial structures in a bone of the Late Cretaceous dinosaur *Saurolophus angustirostris* from the Gobi Desert, Mongolia — a Raman spectroscopy study. *Palaeogeogr. Palaeoclimatol. Palaeoecol.* 358–360, 51–61. doi: 10.1016/j.palaeo.2012.07.020

Kwon, C. W., Ko, K., Gihm, Y. S., Koh, H. J., and Kim, H. (2017). Late Cretaceous volcanic arc system in southwest Korea: distribution, lithology, age, and tectonic implications. *Cretac. Res.* 75, 125–140. doi: 10.1016/j.cretres.2017.03.010

Lahfid, A., Beyssac, O., Deville, E., Negro, F., Chopin, C., and Goffé, B. (2010). Evolution of the Raman spectrum of carbonaceous material in low-grade metasediments of the Glarus Alps (Switzerland). *Terra Nova* 22, 354–360. doi: 10.1111/j.1365-3121.2010.00956.x

Lawver, D. R., and Jackson, F. D. (2014). A review of the fossil record of turtle reproduction: eggs, embryos, nests and copulating pairs. *Bull. Peabody Mus. Nat. Hist.* 55, 215–236. doi: 10.3374/014.055.0210

Lee, S. K., Han, R., Kim, E. J., Jeong, G. Y., Khim, H., and Hirose, T. (2017). Quasi- equilibrium melting of quartzite upon extreme friction. *Nat. Geosci.* 10, 436–441. doi: 10.1038/ngeo2951

Lee, Y.-C., Chiang, C.-C., Huang, P.-Y., Chung, C.-Y., Huang, T. D., Wang, C.-C., et al. (2017). Evidence of preserved collagen in an Early Jurassic sauropodomorph dinosaur revealed by synchrotron FTIR microspectroscopy. *Nat. Commun.* 8:14220. doi: 10.1038/ncomms14220

López-Martínez, N., and Vicens, E. (2012). A new peculiar dinosaur egg, *Sankofa pyrenaica* oogen. nov. oosp. nov. from the Upper Cretaceous coastal deposits of the Aren Formation, south-central Pyrenees, Lleida, Catalonia, Spain. *Palaeontology* 55, 325–339. doi: 10.1038/ncomms1031

Magnabosco, C., Lin, L.-H., Dong, H., Bomberg, M., Ghiorse, W., Stan-Lotter, H., et al. (2018). The biomass and biodiversity of the continental subsurface. *Nat. Geosci.* 11, 707–717. doi: 10.1038/s41561-018-0221-6

Marshall, C. P., Edwards, H. G. M., and Jehlicka, J. (2010). Understanding the application of Raman spectroscopy to the detection of traces of life. *Astrobiology* 10, 229–243. doi: 10.1089/ast.2009.0344

Marshall, C. P., Javaux, E. J., Knoll, A. H., and Walter, M. R. (2005). Combined micro- Fourier transform infrared (FTIR) spectroscopy and micro-Raman spectroscopy of Proterozoic acritarchs: a new approach to Palaeobiology. *Precambrian Res.* 138, 208–224. doi: 10.1016/j.precamres.2005.05.006

Marshall, C. P., Mar, G. L., Nicoll, R. S., and Wilson, M. A. (2001). Organic geochemistry of artificially matured conodonts. *Org. Geochem.* 32, 1055–1071. doi: 10.1016/s0146-6380(01)00077-8

Marzola, M., Russo, J., and Mateus, O. (2015). Identification and comparison of modern and fossil crocodilian eggs and eggshell structures. *Hist. Biol.* 27, 115–133. doi: 10.1080/08912963.2013.871009

Matsumoto, R., and Evans, S. E. (2010). Choristoderes and the freshwater assemblages of Laurasia. *J. Iber. Geol.* 36, 253–274. doi: 10.5209/rev_jige.2010.v36.n2.11

Matsumoto, R., Dong, L., Wang, Y., and Evans, S. E. (2019a). The first record of a nearly complete choristodere (Reptilia: Diapsida) from the Upper Jurassic of Hebei Province, People's Republic of China. *J. Syst. Palaeontol.* 17, 1031–1048. doi: 10.1080/14772019.2018.1494220

Matsumoto, R., Tsogtbaatar, K., Ishigaki, S., Tsogtbaatar, C., Enkhtaivan, Z., and Evans, S. E. (2019b). Revealing body proportions of the enigmatic choristodere reptile *Khurendukhosaurus* from Mongolia. *Acta Palaeontol. Pol.* 64, 363–377. doi: 10.4202/app.00561.2018

McMillan, R., and Golding, M. (2019). Thermal maturity of carbonaceous material in conodonts and the Color Alteration Index: Independently identifying maximum temperature with Raman spectroscopy. *Palaeogeogr. Palaeoclimatol. Palaeoecol.* 534:109290. doi: 10.1016/j.palaeo.2019.109290

McNeil, D. H., Schulze, H. G., Matys, E., and Bosak, T. (2015). Raman spectroscopic analysis of carbonaceous matter and silica in the test walls of recent and fossil agglutinated foraminifera. *AAPG Bull.* 99, 1081–1097. doi: 10.1306/12191414093

Mikhailov, K. E. (1997). Fossil and recent eggshells in amniotic vertebrates: fine structure, comparative morphology and classification. *Spec. Pap. Palaeontol.* 56, 1–80.

Montanari, S. (2018). Cracking the egg: the use of modern and fossil eggs for ecological, environmental and biological interpretation. *R. Soc. Open Sci.* 5:180006. doi: 10.1098/rsos.180006

Montanari, S., Higgins, P., and Norell, M. A. (2013). Dinosaur eggshell and tooth enamel geochemistry as an indicator of Mongolian Late Cretaceous paleoenvironments. *Palaeogeogr. Palaeoclimatol. Palaeoecol.* 370, 158–166. doi: 10.1016/j.palaeo.2012.12.004

Moreno-Azanza, M., Bauluz, B., Canudo, J. I., Gasca, J. M., and Torcida Fernández-Baldor, F. (2016). Combined use of electron and light microscopy techniques reveals false secondary shell units in Megaloolithidae eggshells. *PLoS One* 11:e0153026. doi: 10.1371/journal.pone.0153026

Moreno-Azanza, M., Bauluz, B., Canudo, J. I., Puértolas-Pascual, E., and Sellés, A. G. (2014a). A re-evaluation of aff. Megaloolithidae eggshell fragments from the uppermost Cretaceous of the Pyrenees and implications for crocodylomorph eggshell structure. *Hist. Biol.* 26, 195–205. doi: 10.1080/08912963.2013.786067

Moreno-Azanza, M., Canudo, J. I., and Gasca, J. M. (2014b). Spheroolithid eggshells in the Lower Cretaceous of Europe. Implications for eggshell evolution in ornithischian dinosaurs. *Cretac. Res.* 51, 75–87. doi: 10.1016/j.cretres.2014.05.017

Moreno-Azanza, M., Canudo, J. I., and Gasca, J. M. (2015). Enigmatic Early Cretaceous ootaxa from Western Europe with signals of extrinsic eggshell degradation. *Cretac. Res.* 56, 617–627. doi: 10.1016/j.cretres.2015.06.019

Moreno-Azanza, M., Mariani, E., Bauluz, B., and Canudo, J. I. (2013). Growth mechanisms in dinosaur eggshells: an insight from electron backscatter diffraction. *J. Vert. Paleontol.* 33, 121–130. doi: 10.1080/02724634.2012.710284

Mueller-Töwe, I. J., Sander, P. M., Schüller, H., and Thies, D. (2002). Hatching and infilling of dinosaur eggs as revealed by computed tomography. *Palaeontogr. Abt. A* 267, 119–168.

Nys, Y., Gautron, J., Garcia-Ruiz, J. M., and Hincke, M. T. (2004). Avian eggshell mineralization: biochemical and functional characterization of matrix proteins. *C. R. Palevol.* 3, 549–562. doi: 10.1016/j.crpv.2004.08.002

Olcott Marshall, A., and Marshall, C. P. (2015). Vibrational spectroscopy of fossils. *Palaeontology* 58, 201–211. doi: 10.1111/pala.12144

Oskam, C. L., Haile, J., McLay, E., Rigby, P., Allentoft, M. E., Olsen, M. E., et al. (2010). Fossil avian eggshell preserves ancient DNA. *Proc. R. Soc. B* 277, 1991–2000. doi: 10.1098/rspb.2009.2019

Oskam, C. L., Jacomb, C., Allentoft, M. E., Walter, R., Scofield, R. P., Haile, J., et al. (2011). Molecular and morphological analyses of avian eggshell excavated from a late thirteenth century earth oven. *J. Archaeol. Sci.* 38, 2589–2595. doi: 10.1016/j.jas.2011.05.006

Owocki, K., Kremer, B., Wrzosek, B., Królikowska, A., and Kaźmierczak, J. (2016). Fungal ferromanganese mineralisation in Cretaceous dinosaur bones from the Gobi Desert, Mongolia. *PLoS One* 11:e0146293. doi: 10.1371/journal.pone.0146293

Packard, M. J., and DeMarco, V. G. (1991). "Eggshell structure and formation in eggs of oviparous reptiles," in *Egg Incubation: Its Effects on Embryonic Development in Birds and Reptiles*, eds D. C. Deeming, and M. W. J. Ferguson, (Cambridge: Cambridge University Press), 53–69.

Pan, Y., Sha, J., Zhou, Z., and Fürsich, F. T. (2013). The Jehol Biota: definition and distribution of exceptionally preserved relicts of a continental Early Cretaceous ecosystem. *Cretac. Res.* 44, 30–38. doi: 10.1016/j.cretres.2013.03.007

Pasteris, J. D., and Wopenka, B. (2003). Necessary, but not sufficient: Raman identification of disordered carbon as a signature of ancient life. *Astrobiology* 3, 727–738. doi: 10.1089/153110703322736051

Pérez-Huerta, A., Coronado, I., and Hegna, T. A. (2018). Understanding biomineralization in the fossil record. *Earth-Sci. Rev.* 179, 95–122. doi: 10.1016/j.earscirev.2018.02.015

Piga, G., Santos-Cubedo, A., Brunetti, A., Piccinini, M., Malgosa, A., Napolitano, E., et al. (2011). A multi-technique approach by XRD, XRF, FT-IR to characterize the diagenesis of dinosaur bones from Spain. *Palaeogeogr. Palaeoclimatol. Palaeoecol.* 310, 92–107. doi: 10.1016/j.palaeo.2011.05.018

Quinn, B. (1994). "Fossilized eggshell preparation," in *Vertebrate Paleontological Techniques*, eds P. Leiggi, and P. May, (New York, NY: Cambridge University Press), 146–153.

Rahl, J. M., Anderson, K. M., Brandon, M. T., and Fassoulas, C. (2005). Raman spectroscopic carbonaceous material thermometry of low-grade metamorphic rocks: calibration and application to tectonic exhumation in Crete, Greece. *Earth Planet. Sci. Lett.* 240, 339–354. doi: 10.1016/j.epsl.2005.09.055

Russo, J., Mateus, O., Marzola, M., and Balbino, A. (2017). Two new ootaxa from the Late Jurassic: the oldest record of crocodylomorph eggs, from the Lourinhã Formation, Portugal. *PLoS One* 12:e0171919. doi: 10.1371/journal.pone.0171919

Ryu, I.-C., and Lee, C. (2017). Intracontinental mantle plume and its implications for the Cretaceous tectonic history of East Asia. *Earth Planet. Sci. Lett.* 479, 206–218. doi: 10.1016/j.epsl.2017.09.032

Sadezky, A., Muckenhuber, H., Grothe, H., Niessner, R., and Pöschl, U. (2005). Raman microspectroscopy of soot and related carbonaceous materials: spectral analysis and structural information. *Carbon* 43, 1731–1742. doi: 10.1016/j.carbon.2005.02.018

Saitta, E. T., Fletcher, I., Martin, P., Pittman, M., Kaye, T. G., True, L. D., et al. (2018). Preservation of feather fibers from the Late Cretaceous dinosaur *Shuvuuia deserti* raises concern about immunohistochemical analyses on fossils. *Org. Geochem.* 125, 142–151. doi: 10.1016/j.orggeochem.2018.09.008

Saitta, E. T., Kaye, T. G., and Vinther, J. (2019a). Sediment-encased maturation: a novel method for simulating diagenesis in organic fossil preservation. *Palaeontology* 62, 135–150. doi: 10.1111/pala.12386

Saitta, E. T., Liang, R., Lau, M. C. Y., Brown, C. M., Longrich, N. R., Kaye, T. G., et al. (2019b). Cretaceous dinosaur bone contains recent organic material and provides an environment conducive to microbial communities. *eLife* 8:e46205. doi: 10.7554/eLife.46205

Sander, P. M. (2012). Reproduction in early amniotes. *Science* 337, 806–808. doi: 10.1126/science.1224301

Schidlowski, M. (2001). Carbon isotopes as biogeochemical recorders of life over 3.8 Ga of Earth history: evolution of a concept. *Precambrian Res.* 106, 117–134. doi: 10.1016/s0301-9268(00)00128-5

Schiffbauer, J. D., Wallace, A. F., Hunter, J. L. Jr., Kowalewski, M., Bodnar, R. J., and Xiao, S. (2012). Thermally-induced structural and chemical alteration of organic-walled microfossils: an experimental approach to understanding fossil preservation in metasediments. *Geobiology* 10, 402–423. doi: 10.1111/j.1472-4669.2012.00332.x

Schito, A., Romano, C., Corrado, S., Grigo, D., and Poe, B. (2017). Diagenetic thermal evolution of organic matter by Raman spectroscopy. *Org. Geochem.* 106, 57–67. doi: 10.1016/j.orggeochem.2016.12.006

Schleich, H. H., and Kästle, W. (1988). *Reptile Egg-Shells SEM Atlas*. Stuttgart: Gustav Fischer Verlag.

Schopf, J. W., Kudryavtsev, A. B., Agresti, D. G., Czaja, A. D., and Wdowiak, T. J. (2005). Raman imagery: a new approach to assess the geochemical maturity and biogenicity of permineralized Precambrian fossils. *Astrobiology* 5, 333–371. doi: 10.1089/ast.2005.5.333

Schweitzer, M. H., Avci, R., Collier, T., and Goodwin, M. B. (2008). Microscopic, chemical and molecular methods for examining fossil preservation. *C. R. Palevol.* 7, 159–184. doi: 10.1016/j.crpv.2008.02.005

Schweitzer, M. H., Chiappe, L., Garrido, A. C., Lowenstein, J. M., and Pincus, S. H. (2005). Molecular preservation in Late Cretaceous sauropod dinosaur eggshells. *Proc. R. Soc. B* 272, 775–784. doi: 10.1098/rspb.2004.2876

Silyn-Roberts, H., and Sharp, R. M. (1986). Crystal growth and the role of the organic network in eggshell biomineralization. *Proc. R. Soc. B* 227, 303–324. doi: 10.1098/rspb.1986.0025

Skawiński, T., and Tałanda, M. (2014). Integrating developmental biology and the fossil record of reptiles. *Int. J. Dev. Biol.* 58, 949–959. doi: 10.1387/ijdb.140322mt

Smith, D. L., and Hayward, J. L. (2010). Bacterial decomposition of avian eggshell: a taphonomic experiment. *Palaios* 25, 318–326. doi: 10.2110/palo.2009.p09-115r

Smith, G. D., and Clark, R. J. H. (2004). Raman microscopy in archaeological science. *J. Archaeol. Sci.* 31, 1137–1160. doi: 10.1016/j.jas.2004.02.008

Song, Y., Stepashko, A. A., and Ren, J. (2015). The Cretaceous climax of compression in Eastern Asia: age 87–89 Ma (late Turonian/Coniacian), Pacific cause, continental consequences. *Cretac. Res.* 55, 262–284. doi: 10.1016/j.cretres.2015.01.002

Srivastava, R., Patnaik, R., Shukla, U. K., and Sahni, A. (2015). Crocodilian nest in a Late Cretaceous sauropod hatchery from the type Lameta Ghat locality, Jabalpur, India. *PLoS One* 10:e0144369. doi: 10.1371/journal.pone.0144369

Stein, K., Prondvai, E., Huang, T., Baele, J.-M., Sander, P. M., and Reisz, R. (2019). Structure and evolutionary implications of the earliest (Sinemurian, Early Jurassic) dinosaur eggs and eggshells. *Sci. Rep.* 9:4424. doi: 10.1038/s41598-019-40604-8

Taira, A. (2001). Tectonic evolution of the Japanese island arc system. *Annu. Rev. Earth Planet. Sci.* 29, 109–134. doi: 10.1146/annurev.earth.29.1.109

Tanaka, K., Zelenitsky, D. K., and Therrien, F. (2015). Eggshell porosity provides insight on evolution of nesting dinosaurs. *PLoS One* 10:e0142829. doi: 10.1371/journal.pone.0142829

Tanaka, K., Zelenitsky, D. K., Williamson, T., Weil, A., and Therrien, F. (2011). Fossil eggshells from the Upper Cretaceous (Campanian) Fruitland Formation, New Mexico. *Hist. Biol.* 23, 41–55. doi: 10.1080/08912963.2010.499171

Thomas, D. B., McGoverin, C. M., Fordyce, R. E., Frew, R. D., and Gordon, K. C. (2011). Raman spectroscopy of fossil apatite – a proxy for diagenetic alteration of the oxygen isotope composition. *Palaeogeogr. Palaeoclimatol. Palaeoecol.* 310, 62–70. doi: 10.1016/j.palaeo.2011.06.016

Tuinstra, F., and Koenig, J. L. (1970). Raman spectrum of graphite. *J. Chem. Phys.* 53, 1126–1130. doi: 10.1063/1.1674108

Van Horne, A., Sato, H., and Ishiyama, T. (2017). Evolution of the Sea of Japan back-arc and some unsolved issues. *Tectonophysics* 710–711, 6–20. doi: 10.1016/j.tecto.2016.08.020

Varricchio, D. J., and Jackson, F. D. (2016). Reproduction in Mesozoic birds and evolution of the modern avian reproductive mode. *Auk* 133, 654–684. doi: 10.1642/auk-15-216.1

Wiemann, J., Yang, T.-R., and Norell, M. A. (2018). Dinosaur egg colour had a single evolutionary origin. *Nature* 563, 555–558. doi: 10.1038/s41586-018-0646-5

Yang, T.-R., Chen, Y.-H., Wiemann, J., Spiering, B., and Sander, P. M. (2018). Fossil eggshell cuticle elucidates dinosaur nesting ecology. *PeerJ* 6:e5144. doi: 10.7717/peerj.5144

Yang, T.-R., Wiemann, J., Xu, L., Cheng, Y.-N., Wu, X.-C., and Sander, P. M. (2019). Reconstruction of oviraptorid clutches illuminates their unique nesting biology. *Acta Palaeontol. Pol.* 64, 581–596. doi: 10.4202/app.00497.2018

Yi, S., Lee, Y.-N., and Lee, S.-J. (2004). Palynofacies of the Cretaceous sediments in the Tando Basin, West Korea: thermal maturation and its geological implication. *J. Geol. Soc. Korea* 40, 431–439. (in Korean with English abstract).

Yi, S., Yun, H., and Lee, J.-D. (1998). Palynofacies of the Sansudong Formation (Lower Cretaceous), Jinan Basin, Korea. *J. Paleontol. Soc. Korea* 14, 1–13.

Zhai, M. G., Zhang, Y.-B., Zhang, X. H., Wu, F. Y., Peng, P., Li, Q. L., et al. (2016). Renewed profile of the Mesozoic magmatism in Korean Peninsula: regional correlation and broader implication for cratonic destruction in the North China Craton. *Sci. China Earth Sci.* 59, 2355–2388. doi: 10.1007/s11430-016-0107-0

Zhang, S.-H., Zhao, Y., Davis, G. A., Ye, H., and Wu, F. (2014). Temporal and spatial variations of Mesozoic magmatism and deformation in the North China Craton: implications for lithospheric thinning and decratonization. *Earth-Sci. Rev.* 131, 49–87. doi: 10.1016/j.earscirev.2013.12.004

Zhang, Y.-B., Zhai, M., Hou, Q.-L., Li, T.-S., Liu, F., and Hu, B. (2012). Late Cretaceous volcanic rocks and associated granites in Gyeongsang Basin, SE Korea: their chronological ages and tectonic implications for cratonic destruction of the North China Craton. *J. Asian Earth Sci.* 47, 252–264. doi: 10.1016/j.jseaes.2011.12.011

Conflict of Interest: The authors declare that the research was conducted in the absence of any commercial or financial relationships that could be construed as a potential conflict of interest.